RESEARCH ARTICLE

The FASEB Journal

Compound heterozygous RYR1-RM mouse model reveals disease pathomechanisms and muscle adaptations to promote postnatal survival

Chen Liang[1] | Sundeep Malik[1] | Miao He[1] | Linda Groom[1] | Sara K. Ture[2] | Thomas N. O'Connor[1] | Craig N. Morrell[2] | Robert T. Dirksen[1]

[1]Department of Pharmacology and Physiology, University of Rochester Medical Center, Rochester, New York, USA

[2]Department of Medicine, Cardiovascular Research Institute, University of Rochester, Rochester, New York, USA

Correspondence
Robert T. Dirksen, Department of Pharmacology and Physiology, University of Rochester Medical Center, 601 Elmwood Avenue, Rochester, NY 14642, USA.
Email: robert_dirksen@urmc.rochester.edu

Abstract

Pathogenic variants in the type I ryanodine receptor (RYR1) result in a wide range of muscle disorders referred to as RYR1-related myopathies (RYR1-RM). We developed the first RYR1-RM mouse model resulting from co-inheritance of two different RYR1 missense alleles ($Ryr1^{TM/SC-\Delta L}$ mice). $Ryr1^{TM/SC-\Delta L}$ mice exhibit a severe, early onset myopathy characterized by decreased body/muscle mass, muscle weakness, hypotrophy, reduced RYR1 expression, and unexpectedly, incomplete postnatal lethality with a plateau survival of ~50% at 12 weeks of age. $Ryr1^{TM/SC-\Delta L}$ mice display reduced respiratory function, locomotor activity, and in vivo muscle strength. *Extensor digitorum longus* muscles from $Ryr1^{TM/SC-\Delta L}$ mice exhibit decreased cross-sectional area of type IIb and type IIx fibers, as well as a reduction in number of type IIb fibers. Ex vivo functional analyses revealed reduced Ca^{2+} release and specific force production during electrically-evoked twitch stimulation. In spite of a ~threefold reduction in RYR1 expression in single muscle fibers from $Ryr1^{TM/SC-\Delta L}$ mice at 4 weeks and 12 weeks of age, RYR1 Ca^{2+} leak was not different from that of fibers from control mice at either age. Proteomic analyses revealed alterations in protein synthesis, folding, and degradation pathways in the muscle of 4- and 12-week-old $Ryr1^{TM/SC-\Delta L}$ mice, while proteins involved in the extracellular matrix, dystrophin-associated glycoprotein complex, and fatty acid metabolism were upregulated in $Ryr1^{TM/SC-\Delta L}$ mice that survive to 12 weeks of age. These findings suggest that adaptations that optimize RYR1 expression/Ca^{2+} leak balance, sarcolemmal stability, and fatty acid biosynthesis provide $Ryr1^{TM/SC-\Delta L}$ mice with an increased survival advantage during postnatal development.

KEYWORDS
calcium signaling, congenital myopathy, excitation-contraction coupling, proteomics, ryanodine receptor, skeletal muscle

---

Abbreviations: CCD, central core disease; CPA, cyclopiazonic acid; CSA, cross sectional area; DHPR, dihydropyridine receptor; EC, excitation–contraction; EDL, extensor digitorum longus; EF50, Mid-expiratory flow; F, ventilatory frequency; FDB, flexor digitorum brevis; LO, optimal length; MH, malignant hyperthermia; RYR1, Type I ryanodine receptor; RYR1-RM, RYR1-related myopathies; SR, sarcoplasmic reticulum; TA, Tibialis anterior; TBS, tris-buffered saline; VE, minute volume; VT, tidal volume.

---

1 | INTRODUCTION

Congenital myopathies result from mutations in over 20 genes that encode proteins involved in skeletal muscle Ca^{2+} homeostasis, excitation–contraction (EC) coupling, and sarcomere assembly/function. Among all the congenital myopathies, variants in the gene that encodes the type I ryanodine receptor (*RYR1*), which forms the Ca^{2+} release channel of the sarcoplasmic reticulum (SR),[1] represent the most frequent subgroup.[2,3] RYR1-related myopathies result from a broad range of variants, which exhibit both dominant and recessive modes of inheritance, thus resulting in great variability in phenotypic presentation.[3–5] Most cases of dominantly inherited RYR1-related disorders result from missense variants that are associated with increased susceptibility to malignant hyperthermia, exertional rhabdomyolysis, and/or central core disease.[6] Typically, recessively inherited RYR1-related disorders, including multi-minicore disease, centronuclear myopathy, and congenital fiber type disproportion, exhibit an earlier onset and a more clinically severe presentation.[7–10] For example, children with recessively inherited RYR1-RM (RYR1-RM) can be non-ambulant, require ventilator assistance, and experience severe disability, and even premature death.[4,5] Despite this significant disability and early mortality, there are currently no effective treatments or disease-modifying therapies for individuals with recessive RYR1-RM.

Although clustering of disease variants within specific regions of the RYR1 sequence has been reported (e.g., many dominant CCD variants are located in the RYR1 C-terminal region), dominant and recessive RYR1 variants are distributed throughout the linear RYR1 amino acid sequence.[11–14] Typically, dominant MHS variants enhance RYR1 sensitivity to activation, while dominant CCD variants lead to reduced SR Ca^{2+} release by either promoting uncompensated RYR1 Ca^{2+} leak or reducing RYR1 Ca^{2+} permeability.[11–14] There are three forms of recessively inherited RYR1-RM: (1) bi-allelic (homozygous) missense variant, (2) monoallelic expression of a missense variant in combination with a hypomorphic allele (e.g., nonsense or frameshift variant), and (3) compound heterozygous missense variants.[11–14] This diversity of recessive RYR1 disease inheritance patterns ultimately leads to the formation of tetrameric SR Ca^{2+} release channels with complex stoichiometry (homotypic variant channels and compound variant heterotetrameric channels), levels of expression (normal vs. reduced RYR1 expression), and altered function (sensitivity to activation, Ca^{2+} leak, and Ca^{2+} permeability). Thus, pathophysiological mechanisms resulting from these different inherited forms of recessive RYR1-RM, and the precise relationships of the specific RYR1 variants involved, are not fully understood.

As a result, a comprehensive understanding of the genotype–phenotype relationships requires careful dissection of the underlying pathophysiological mechanisms using appropriate mouse models for each of the three different forms of recessive RYR1-RM.

Mouse models of recessive RYR1-RM exhibit remarkably distinct phenotypes.[11–15] For example, two different models of recessive RYR1-RM based on co-inheritance of a missense variant allele coupled with a frameshift hypomorphic allele (Ryr1p.R4704fsX16+p.T4706M or TM/Indel; Ryr1p.Q1970fsX16+p.A4329D or AD/Indel) similarly exhibit reduced muscle/body mass, myofiber cross-sectional area, and levels of both RYR1 transcript (~50%) and protein (70%–80%).[11,12] In spite of these similarities, overall disease severity between these two models of recessive RYR1-RM is remarkably different. While AD/Indel mice live well into adulthood, all TM/Indel mice die within the first 2 months of postnatal development. As AD/Indel mice age, they develop a core phenotype characterized by myofibrillar and mitochondrial disorganization, and treatment of these mice with inhibitors of DNA methylase and class II histone deacetylase enzymes improves muscle strength, RYR1 protein content, and ultrastructure.[16]

Several different mouse models of homozygous recessive RYR1-RM have also been reported. Mice homozygous for the T4706M variant (TM/TM) exhibit normal body mass and live into adulthood. However, TM/TM mice do exhibit signs of a mild, late-onset myopathy exemplified by the development of kyphosis, a modest reduction in muscle RYR1 expression, and an increased sensitivity to exposure to volatile anesthetics (e.g., isoflurane).[11] In addition, a fraction of RYR1 channels isolated from TM/TM mice exhibit high open probability under conditions of both physiologic (100 nM) and high (50 μM) cytoplasmic concentrations of Ca^{2+}, thus resulting in essentially Ca^{2+}-insensitive, constitutively high P_O (or leaky) RYR1 channels.[17] Mice homozygous for the AD variant (AD/AD) similarly exhibit a milder phenotype than that observed for AD/Indel mice.[12] A recent study reported that mice homozygous for a F4976L variant (FL/FL) exhibit a relatively mild myopathy due to a relatively modest reduction in RYR1 expression (10%–20%), increase in RYR1 Ca^{2+} leak, as well as a decrease in both electrically evoked Ca^{2+} release and force production.[15] Although technically not a murine model of recessive RYR1-RM, Pelletier et al. used inducible, muscle-specific *RYR1* knockdown mice to demonstrate significant muscle weakness, atrophy, and a core-like myopathy when RYR1 expression is reduced ~50% in adult mice compared to that of age-matched wild type mice.[14]

While these mouse models provide valuable insights into the disease pathomechanisms that underlie

the homotypic expression of a given RYR1 variant, co-inheritance of missense and hypomorphic variants and reduced RYR1 expression in adulthood, there are no mouse models of human RYR1-RM resulting from co-inheritance of two different missense *RYR1* alleles. To address this unmet need, we generated a recessive compound missense mouse model based on an individual with recessive RYR1-RM arising from a paternal *RYR1* allele with a single missense variant in exon 96 (T4709M) and a maternal *RYR1* allele with two missense variants in exon 34 (R1667C and ΔL1714).[18] While both parents are clinically asymptomatic (though the father exhibits statin intolerance), their son was diagnosed with a recessive RYR1-RM characterized by myopathic histopathology (i.e., myofiber diameter variability, reduced mitochondrial content, and cores) and progressive muscle weakness resulting in impaired ambulation.[18] To model this recessive form of RYR1-RM, we used separate knock-in mouse lines for the corresponding murine missense variants in exon 96 (T4706M or $Ryr1^{TM/+}$) and exon 34 (S1669C and ΔL1716 or $Ryr1^{SC-ΔL/+}$). Results obtained from compound heterozygous mice produced by intercrossing these two parental lines ($Ryr1^{TM/SC-ΔL}$ mice) provide important insights into both the underlying disease pathomechanisms and muscle adaptations designed to promote postnatal survival.

2 | MATERIALS AND METHODS

2.1 | Animals

The parental $Ryr1^{TM/+}$ and $Ryr1^{SC-ΔL/+}$ mouse lines generated in a congenic C57Bl6 background by Ingenious Targeting Laboratory using conventional homologous recombination methods were kindly provided by the RYR-1 Foundation. $Ryr1^{TM/+}$ mice possess a point mutation in exon 96 (T4706M or TM) and $Ryr1^{SC-ΔL/+}$ mice possess two in-frame mutations in exon 34 (S1669C and L1716Del or SC-ΔL). Briefly, each parental line was generated using a neomycin selection cassette flanked by an FRT site in iTL BF1 (C57BL/6 FLP). Embryonic stem cells were microinjected into Balb/c blastocysts in order to establish a germline of chimeric mice. Once the selection cassette was removed by introducing a site-specific recombinase FLP, neomycin-deleted mice were generated and then crossed with WT mice to generate heterozygous neomycin-deleted mice. The two parental lines were continually maintained by backcrossing with congenic C57Bl6 mice obtained from Jackson Laboratories. Neither $Ryr1^{TM/+}$ nor $Ryr1^{SC-ΔL/+}$ mice exhibited an overt phenotype and both mouse strains thrive and live well into adulthood. Compound heterozygous $Ryr1^{TM/SC-ΔL}$ mice were generated by intercrossing the two parental lines. All mice were weaned at 4 weeks of age and housed in microisolator cages at 20°C on a 12-h light/dark cycle while being provided ad libitum access to standard chow and water. $Ryr1^{TM/SC-ΔL}$ mice (4–12 weeks old) were also provided with extra Nutra-Gel Diet and weekly teeth trimming care due to the development of malocclusions. Inclusion criteria included age, sex, and genotype. As no overt sex-dependent differences were observed for $Ryr1^{SC-ΔL/+}$ mice, male and female mice were used and combined for all experiments. Except for premature death, no animals were identified for attrition. All animal procedures followed protocols that were approved by the University Committee on Animal Resources at the University of Rochester (protocol number UCAR-2006-114E).

2.2 | Whole-body plethysmography

To evaluate respiratory function of $Ryr1^{TM/SC-ΔL}$ mice, respiratory flow recordings were performed using whole-body plethysmography in unrestrained, unanesthetized mice during eupnea. Following calibration according to the manufacturer's recommendations, animals were placed into plethysmograph chambers (Buxco Research Systems, Wilmington, NC), acclimated to the chamber for 5 min, and then respiratory function was recorded for 15 min. Respiratory metrics were calculated using Fine Point software (Buxco Research Systems, Wilmington, NC) including ventilatory frequency (F), tidal volume (VT), minute volume (VE), peak inspiratory and expiratory flow rate, and EF_{50} (flow rate at 50% of tidal volume during expiration). For all whole-body plethysmography studies, mice were randomized and experimenters were blinded to mouse genotype during data collection and unblinded following completion of data analyses.

2.3 | In vivo behavioral assessments

2.3.1 | Hang task

A wire hang test was used to evaluate sustained grip strength. Mice were hung from an inverted metal cage for 60 s with the time to fall recorded. Mice able to hang more than 60 s were recorded as 60 s. Average time for each mouse was calculated from three consecutive trials with 5 min of rest between trials.

2.3.2 | Hang and escape

A wire "hang and escape" test was used to evaluate overall mouse muscle core strength and motor coordination.

Briefly, mice grasp a taut horizontal wire at a point equidistant between two supporting platforms located 50 cm apart and 40 cm above a padded surface. Mice were scored (0–5) for their ability to hang from the wire, lift, and escape to one of the two side supports as described previously.[19] A maximum of 60 s was given for each attempt. An average escape score for each mouse was obtained from 10 attempts with 30 s rest between trials.

2.3.3 | Grip strength

In vivo, grip strength was evaluated in mice with all four paws together using an apparatus consisting of a stainless steel grid of 1-cm divisions connected to a precision digital force gauge (GTX; Dillon, Woodlands, TX)[19] set to record peak tensile force. The apparatus was arranged in a horizontal orientation, with the gripping grid placed on a horizontal track that minimizes frictional force. Each mouse was lowered to the apparatus, allowed to grasp the grid, and pulled slowly from their tail continuously away from the force gauge until grip failed. Peak tensile force at the point of grip failure was recorded and normalized by mouse weight (mN/g).

For all in-vivo behavioral studies, mice were randomized and experimenters were blinded to mouse genotype during data collection and unblinded following completion of data analyses.

2.4 | RNA extraction and RT-qPCR

RNA from *tibialis anterior* (TA) muscles was extracted using TRIzol reagent (Life Technology, Calsbad, CA) following the manufacturer's protocol. RNA (1 μg) was treated with DNase (Thermo Fisher Scientific, Waltham, MA) and cDNA libraries were generated using Super Script III First-Strand Synthesis System primed with oligo (dT) (Thermo Fisher Scientific, Waltham, MA). qPCR was performed using qScript™ cDNA SuperMix (Quantabio, Beverly, MA) and a 7500 Fast Real-Time PCR system (Applied Biosystems, Thermo Fisher Scientific, Waltham, MA) with StepOnePlus software to collect and analyze data. *Ryr1* transcript levels were normalized to an average transcript level of *Gapdh*. The following primers were used:

Ryr1 Forward Primer: 5′-ATGACCGTAGGGCTCCTG GCCGTAG-3′
Ryr1 Reverse Primer: 5′-GGGTCCTCGATCTCGTCC CCGA-3′
Gapdh Forward Primer: 5′-AGGTCGGTGTGAACGGA TTTG-3′

Gapdh Reverse Primer: 5′-TGTAGACCATGTAGTTGA GGTCA-3′

2.5 | Western blot analyses

Muscles (TA, *soleus*, *flexor digitorum brevis*, *diaphragm*) were homogenized in RIPA buffer supplemented with Halt protease inhibitor (Thermo Fisher Scientific, Waltham, MA) with protein concentration assessed using the RC/DC protein assay (Bio-Rad, Hercules, CA). Proteins (~2–10 μg) were individually separated by SDS-PAGE via SDS acrylamide gel. Following 2 h of electrophoresis at 100 V, the proteins were transferred to nitrocellulose membranes overnight at 25 V. The membranes were then blocked in 3% bovine serum albumin (BSA) in Tris Buffered Saline with Tween 20 (TBST) for 1 h at room temperature and incubated with a primary antibody overnight at 4°C for Ryr1 (DSHB, Iowa City, IA; 1:30), Dhpr (DSHB, Iowa City, IA; 1:500), Dmd (Abcam, Waltham, MA; 1:500), Fasn (Proteintech, Rosemont, IL; 1:2000), Acly (Proteintech, Rosemont, IL; 1:2000), Sperpina3k (Proteintech, Rosemont, IL; 1:2000), Col3a1 (DHSB, Iowa City, IA; 1:30), Sgca (DHSB, Iowa City, IA; 1:30), and Gapdh (Invitrogen, Waltham MA; 1:50 000) all in 3% BSA in TBST. Following three washes in TBST, blots were incubated with Anti-Mouse or Anti Rabbit IgG800 (Thermo Fisher Scientific, Waltham, MA) at 1:10 000 dilution in 5% nonfat milk in TBST. Membranes were imaged using an Odyssey Infrared imager from LiCor (LI-COR, Lincoln, NE). Proteins were quantified using the Image Studio software from LiCor (LI-COR, Lincoln, NE).

2.6 | Ryr1-Fkbp12 co-immunoprecipitation

TA muscle lysates in RIPA buffer from 12-week-old WT and *Ryr1^{TM/SC-ΔL}* mice were incubated with 2 μg of mouse anti-Ryr1 antibody (#34C, DSHB, Iowa City, IA) and 15 μL of Pierce protein A/G magnetic beads (Thermo Fisher Scientific, Waltham, MA) overnight at 4°C while gently shaking. Beads were separated on a magnetic rack, washed three times with cold RIPA buffer, and the immunoprecipitated (IP) was eluted in 50 μL of Laemmli buffer. Either 5 μg of TA lysate or 10 μL of the IP was loaded in each lane of the gel. For Ryr1, samples were resolved on a 6% SDS-acrylamide gel and the blot was probed with a rabbit anti-Ryr1 antibody (D4E1, Cell Signaling Technology, Danvers, MA). For Fkbp12, samples were resolved on a 16.5% SDS-acrylamide gel and

the blot was probed with a mouse anti-Fkbp12 antibody (H-5, Santa Cruz Biotechnology Inc., Dallas, TX).

2.7 | Cryopreservation and muscle sectioning

Extensor digitorum longus (EDL) and *soleus* muscles were kept in 30% sucrose in PBS solution at 4°C overnight and mounted in optimal cutting temperature medium and snap frozen in 2-methylbutane with dry ice. Muscles were transversally sectioned at $10\,\mu m$ thickness and mounted on SuperFrost Plus slides (Thermo Fisher Scientific, Waltham, MA).

2.8 | Immunofluorescence

Mounted EDL and *soleus* sections were blocked for 30 min in blocking buffer containing 1% Tris-buffered saline (TBS) solution, 0.1% BSA, 10% goat serum, 0.1% Triton X-100 and 0.1% Tween-20 (pH 7.9) followed by AffiniPure Fab Fragment goat anti-mouse IgG (1.0 mg) (JacksonImmuno Research Inc., West Grove, PA). Slides were then incubated with primary antibodies against myosin heavy chain I, IIA, IIB (DSHB, Iowa City, IA), and laminin (Sigma-Aldrich, St. Louis, MA) at 1:1500 and 1:1000, respectively, and subsequently incubated with secondary antibodies goat anti-rabbit Alexa Fluor 488, goat anti-mouse IgG1 cross-adsorbed Ab 555 (Invitrogen, Waltham, MA), goat anti-rabbit IgG H&L 647 (Abcam, Woburn, MA), and goat anti-mouse IgG2b 405S (Sigma-Aldrich, St. Louis, MA). Slides were imaged at 4× magnification using the Keyence BZ-X800 fluorescent microscope (Lumenera Corporation, Ottawa, ON, Canada) equipped with BZ-X800 Viewer software (Keyence Coperation, Itasca, IL). Fiber type and cross-sectional area analyses of immunofluorescence images muscle cross-sections were determined using Smash, a MATLAB-based program developed in Dr. Elizabeth Barton's laboratory.[20]

2.9 | Hematoxylin and eosin staining

EDL muscle sections were stained with hematoxylin and eosin (H&E) and then dehydrated with graded alcohols and xylene. Images were captured at 20× magnification using the Keyence BZ-X800 fluorescent microscope (Lumenera Corporation, Ottawa, ON, Canada) equipped with BZ-X800 Viewer software (Keyence Corporation, Itasca, IL).

2.10 | Ex vivo muscle contractility and fatigability

Excised muscles (EDL, *soleus*, *diaphragm*) were mounted between two platinum electrodes in oxygenated Ringer solution at 30°C with one end connected to a 300C-LR dual mode force transducer. Muscle optimal length (L_O) was determined using a series of twitch tension stimulated by ASI muscle contraction system equipped with a 701C stimulator (Aurora Scientific, Aurora, ON, Canada). Stimulus output was adjusted to 120% of the voltage required to elicit maximal force. All muscles were initially equilibrated using three 500 ms, 150 Hz tetani at 1 min intervals and then subjected to a force-frequency protocol (500 ms tetani, 0.04 duty cycle). Muscle force was recorded using the Dynamic Muscle Control software (Aurora Scientific, Aurora, ON, Canada) and analyzed using Clampfit 10.3 software (Molecular Devices, Sunnyvale, CA). Muscle cross-sectional area (CSA) and specific force were calculated as previously described.[21]

2.11 | Electrically evoked Ca^{2+} release in single FDB fibers

Single *flexor digitorum brevis* (FDB) muscle fibers were dissociated by enzymatic digestion with collagenase A (1 mg/mL) in regular rodent Ringer solution (in mM: 146 NaCl, 5 KCl, 2 MgCl$_2$, 2 CaCl$_2$, and 10 HEPES, pH 7.4) with gentle agitation for 1 h at 37°C. Individual fibers were liberated by gentle tritration. Single fibers were then loaded with $4\,\mu M$ mag-fluo-4 acetoxymethyl ester for 20 min at room temperature followed by washout with a control Ringer's solution supplemented with $25\,\mu m$ benzyl-p-toluene sulfonamide (BTS), a skeletal muscle myosin inhibitor used to minimize movement. Mag-fluo-4-loaded FDB fibers were stimulated with a series of electrically evoked twitch stimulations (1 Hz) or five consecutive tetani (500 ms at 100 Hz) using an extracellular electrode placed adjacent to the cell of interest. Mag-fluo-4 was excited at 480 ± 15 nm using an Excite epifluorescence illumination system (Nikon Instruments, Melville, NY) with fluorescence emission at 535 ± 30 nm monitored with a 40× oil objective and a photomultiplier detection system (Photon Technologies Inc., Birmingham, NJ). Relative changes in mag-fluo-4 fluorescence from baseline (F/F_0) were collected using Clampex 10.0 software (Molecular Devices, San Jose, CA). The decay phase of each transient was fitted according to the following two exponential equation:

$$F(t) = A_{fast} \times \left[\exp\left(-\tau / \tau_{fast} \right) \right] + A_{slow} \times \left[\exp\left(-\tau / \tau_{slow} \right) \right]$$

where $F(t)$ is the fluorescence at time t, A_{fast} and τ_{fast} are the amplitude and time constants of the fast component of decay, which primarily reflects Ca^{2+} binding to fast myoplasmic Ca^{2+} buffers, and A_{slow} and τ_{slow} are the amplitude and time constants of the slow component of decay, which is dominated by SERCA pump-mediated Ca^{2+} reuptake.[22,23]

2.12 | Total releasable Ca^{2+} store content

Single FDB myofibers were loaded with the low-affinity Ca^{2+} dye, fura-FF AM. Fibers were perfused with a Ca^{2+} release cocktail containing 10 μM ionomycin, 30 μM cyclopiazonic acid (CPA), and 100 μM EGTA in a Ca^{2+}-free Ringer's solution (ICE) in order to rapidly and fully deplete intracellular Ca^{2+} stores.[19,24] To confirm that the peak fura-FF signal during ICE application was not saturated, maximal fura-FF responsiveness was assessed at the end of each experiment by subsequent application of Ca^{2+}-containing Ringer's solution. Analyses of peak ICE-induced change in fura-FF ratio (ΔRatio$_{340/380}$) were calculated using Clampfit 10.0 (Molecular Devices, Sunnyvale, CA).

2.13 | SR Ca^{2+} leak

SR Ca^{2+} leak was determined in single FDB myofibers loaded with 5 μM fura-2 AM for 30 min at room temperature in Ca^{2+}-free Ringer's solution followed by 30 min washout in dye-free Ringer's solution, as described previously.[25] Briefly, fura-2-loaded fibers were first perfused in Ca^{2+}-free Ringer's solution supplemented with 40 μM BTS and 100 μM EGTA while alternately being excited at 340 and 380 nm every 250 ms (30 ms exposure per wavelength and 2×2 binning) using a monochromator-based illumination system (TILL Photonics, Graefelfing, Germany). Fibers were then perfused with the same solution supplemented with 30 μM CPA in order to inhibit SERCA-mediated SR Ca^{2+} reuptake. Fura-2 emission at 510 nm was captured using a high-speed, digital QE CCD camera (TILL Photonics, Graefelfing, Germany). The maximum rate of increase in fura-2 emission ratio (340/380) during CPA-mediated SERCA inhibition was used as a quantitative index of the maximum rate of SR Ca^{2+} leak.

2.14 | Resting Ca^{2+} measurements

Resting myoplasmic Ca^{2+} concentration was determined in FDB fibers loaded with 5 μM fura-2 AM for 30 min at room temperature in Ringer's solution followed by a 30 min washout with Ringer's solution. Fura-2-loaded fibers were alternatively excited at 340 and 380 nm (30 ms exposure per wavelength and 2×2 binning) using a monochromator-based illumination system with fura-2 fluorescence emission at 510 nm collected using a high-speed, digital QE CCD camera (TILL Photonics, Graefelfing, Germany). Fura-2 emission ratios (340/380) from myoplasmic areas of interest were calculated using TILL visION software (TILL Photonics, Gräefelfing, Germany) and converted to resting free Ca^{2+} concentrations using an in situ calibration curve for fura-2 generated as described previously.[26]

2.15 | Proteomic analyses

Gastrocnemius muscles from 4-week to 12-week-old male $Ryr1^{+/+}$ and $Ryr1^{TM/SC-\Delta L}$ mice ($n = 4$ each) were excised and homogenized in 5% SDS with 100 mM TEAB using strong ultra-sonication (QSonica, Newtown, CT) for five cycles, with a 1-min rest period on ice after each cycle. Samples were then centrifuged at 15 000 × g for 5 min, and the supernatant was collected for protein concentration determination by BCA assay (Thermo Fisher Scientific, Waltham, MA). After dilution of samples to 1 mg/mL in 5% SDS, 50 mM TEAB, aliquots of 25 μg of protein were reduced with 2 mM dithiothreitol for 60 min at 55°C and alkylated with 10 mM iodoacetamide for 30 min. Samples were then diluted with 1.2% phosphoric acid, 90% methanol, 100 mM TEAB and added to S-Trap micros (Protifi, Fairport, NY), followed by centrifuged at 4000 × g for 1 min, washed, and digested with 1 μg trypsin overnight at 37°C. Samples were then centrifuged and the digested peptides were collected. After sequential acidification by 0.1% TFA in 100% and 50% acetonitrile, samples were frozen and dried down in a Speed Vac (Labconco, Fullerton, CA). Frozen samples were resuspended in 0.1% trifluoroacetic acid prior to mass spectrometry analysis.

Chromatographic separation of peptides was performed using an Easy nLC-1200 HPLC (Thermo Fisher Scientific, Waltham, MA), equipped with a homemade 30 cm C18 column. Aliquots of 1 μg total peptides were analyzed using a linear gradient ranging from 97% solvent A (0.1% formic acid) and 3% solvent B (0.1% formic acid in 80% acetonitrile) to final 90% solvent B over 90 min. Mass spectrometry analyses were performed using a Fusion Lumos Tribrid mass spectrometer (Thermo Fisher Scientific, Waltham, MA) with a Nanospray Flex source operating at 2 kV. MS1 scan was performed at a resolution of 60 000 at 200 m/z over a maximum time of 50 ms. MS2 scans were performed by using higher energy dissociation (HCD), which was

acquired at the setting of accumulation time of 23 ms and a resolution of 15 000 at 200 m/z.

The raw files were analyzed by DIA-NN version 1.8.1 (https://github.com/vdemichev/DIA-NN) using library-free analysis mode, with selected mouse UniProt 'one protein sequence per gene' database (UP000000589_10090, downloaded 4/7/2021). Peptide precursor ion intensities were extracted by applying the following parameters: the maximum number of missed cleavages was set to 1; maximum number of variable modifications was set to 1 for Ox(M); peptide length range was set to 7–30; precursor charge range was set to 2–3; precursor m/z range was set to 400–1000; and fragment m/z range was set to 200–2000. The data quantification was set to 'Robust LC (high precision)' mode with MBR enabled. MS1 and MS2 mass tolerances, along with the scan window size were applied with the default parameters of the software. The results were filtered using library precursor and protein levels set to q-value of 1%, with posterior error probability set to 50%. Protein quantification was performed using the MaxLFQ algorithm as implemented in the DIA-NN R package (https://github.com/vdemichev/diann-rpackage). Peptide quantification was analyzed using the DiannReportGenerator Package (https://github.com/kswovick/DIANN-Report-Generator).

Volcano plots were generated from GraphPad Prism 9.0 with Log_2 fold change set to ±0.5; significance threshold set to $-\text{Log}_{10} > 1.3$.[27] Enrichment analyses were performed using ShinyGO 0.80 with FDR cutoff set at 0.05 and pathway minimum size set at 5 with output of the top 10 Cellular Component GO pathways for significantly increased and decreased proteins organized separately according to fold enrichment.

2.16 | Whole blood collection and analysis

Prior to the collection of whole blood, mice were anesthetized by intraperitoneal injection of ketamine (100 mg/kg) and xylazine (10 mg/kg). Once the mice were at an appropriate anesthetic plane, an EDTA-coated glass capillary tube was introduced into the lateral canthus of the eye. Whole blood was then withdrawn into tubes for subsequent complete blood count analysis using an Abaxis (Zoetis) VetScan HM5 Hematology System (Abaxis Inc., Griesheim, Germany).

2.17 | Statistical analyses

A priori power calculations of sample size based on a standard deviation of our preliminary data, published literature, and investigator experience were used to determine the number of animals required for each experiment. Statistical significance of measurements was assessed by one-way ANOVA followed by post hoc Tukey test for pairwise comparisons between multiple genotypes or a Student's t-test for comparisons between $Ryr1^{TM/SC-\Delta L}$ and $Ryr1^{+/+}$. A significance level of $p < .05$ was selected for all analyses. All summary data were presented as mean ± SEM.

3 | RESULTS

3.1 | $Ryr1^{TM/SC-\Delta L}$ mice exhibit reduced body mass and postnatal survival

3.1.1 | Survival

Survival. Figure 1A (*top*) shows a schematic of the kindred for a compound heterozygous recessive RYR1-RM family due to co-inheritance of two different RYR1 missense variant alleles (paternal T4709M allele and maternal R1667C and ΔL1714 allele). Intercrossing knock-in mouse lines heterozygous for the corresponding murine *Ryr1* missense variants ($Ryr1^{TM/+}$ and $Ryr1^{SC-\Delta L/+}$ mice) results in compound heterozygous RYR1-RM mice ($Ryr1^{TM/SC-\Delta L}$ mice). A representative image of 4-week-old $Ryr1^{+/+}$ and $Ryr1^{TM/SC-\Delta L}$ mice is shown in Figure 1A (*middle*). In contrast to an expected 25%, the birth rate of $Ryr1^{TM/SC-\Delta L}$ mice was only 15.3%, consistent with a modest level of embryonic lethality. The other three genotypes, wild type ($Ryr1^{+/+}$), $Ryr1^{TM/+}$, and $Ryr1^{SC-\Delta L/+}$ mice, all exhibited birth rates at or slightly above the expected 25% (Figure 1A, *bottom*, *inset*). In addition, early postnatal mortality of $Ryr1^{TM/SC-\Delta L}$ mice commences around 4 weeks of age, but interestingly, exhibits a plateau survival of ~50% at 12 weeks of age (Figure 1A, *bottom*). After weaning, $Ryr1^{TM/SC-\Delta L}$ mice displayed diminished mobility, malocclusions, microphthalmia/ocular infections, and kyphoscoliosis. These phenotypic alterations, coupled with reduced cage activity, food consumption, and muscle hypotrophy likely lead to premature death due to a failure to thrive and respiratory insufficiency (see also Figure 2).

3.1.2 | Body and muscle mass

Body and muscle mass. $Ryr1^{TM/SC-\Delta L}$ mice exhibited a significant reduction in body weight as early as 3 days postpartum. Although the initial reduction in body weight of $Ryr1^{TM/SC-\Delta L}$ compared to the other genotypes was modest, this reduction increased further over the ensuing month (Figure 1B). By the end of the first month, $Ryr1^{TM/SC-\Delta L}$ mice exhibited a body weight of approximately ~50% of that observed for the other genotypes, which continued
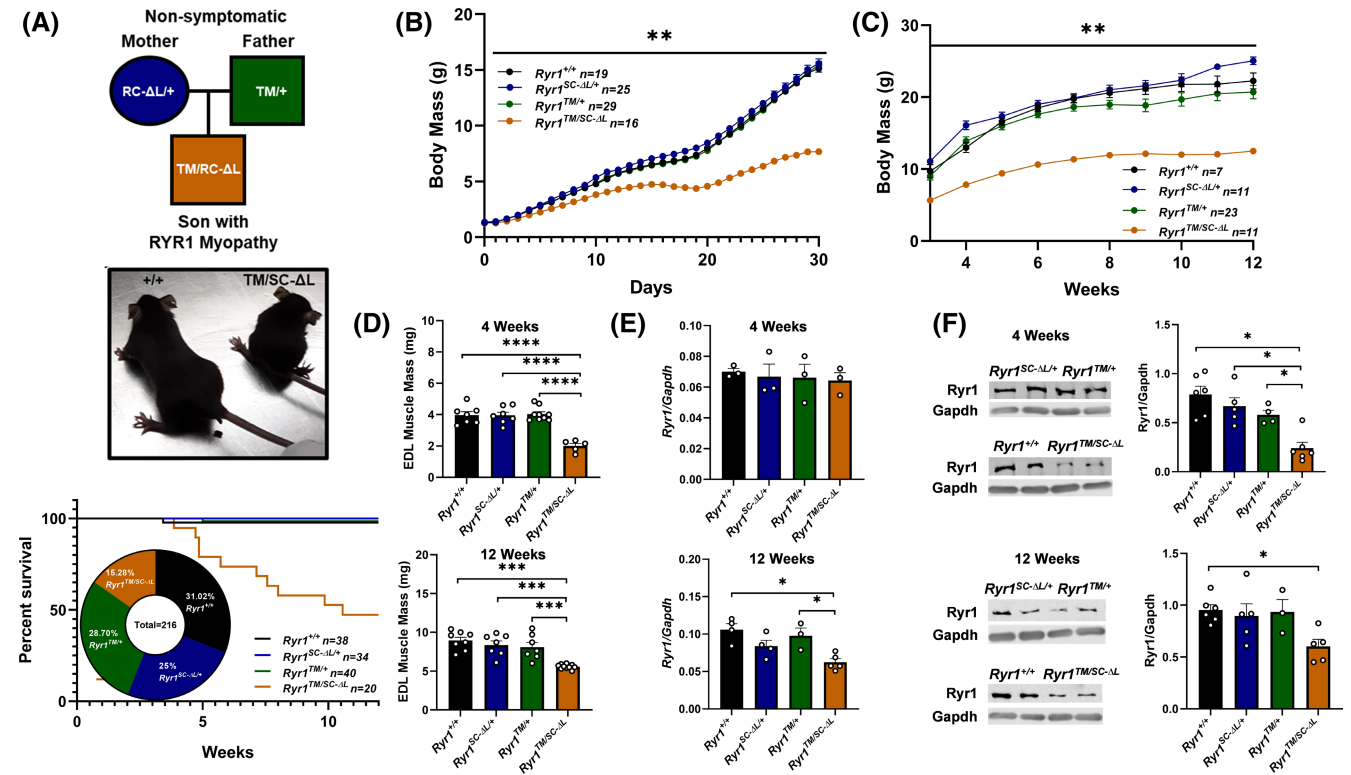
FIGURE 1 $Ryr1^{TM/SC-\Delta L}$ mice exhibit a decline in birth rate, postnatal survival, body weight, muscle mass, and Ryr1 protein expression. (A) Kindred schematic of a compound heterozygous recessive RYR1-RM family due to co-inheritance of two different *RYR1* missense variant alleles (paternal T4909M allele and maternal R1667C and ΔL1714 allele) (*top*). Representative image of 4-week-old $Ryr1^{+/+}$ and $Ryr1^{TM/SC-\Delta L}$ mice (*middle*). $Ryr1^{TM/SC-\Delta L}$ mice exhibit reduced birth and postnatal survival rates, with only ~50% of mice surviving to 12 weeks of age (*bottom*). (B) Reduced body weight of $Ryr1^{TM/SC-\Delta L}$ mice during the first 4 weeks after birth. (C) Reduced body weight of $Ryr1^{TM/SC-\Delta L}$ mice continues from 4 to 12 weeks of age, during a time when ~50% of $Ryr1^{TM/SC-\Delta L}$ mice die. (D) EDL muscle mass of $Ryr1^{TM/SC-\Delta L}$ mice is significantly reduced at both 4 weeks (*top*) and 12 weeks of age (*bottom*). (E) $Ryr1^{TM/SC-\Delta L}$ mice exhibit a significantly reduced level of *Ryr1* transcript at 12 weeks of age (*bottom*), but not at 4 weeks of age (*top*). (F) $Ryr1^{TM/SC-\Delta L}$ mice exhibit a significantly reduced Ryr1 protein expression at both 4 weeks of age (*top*) and 12 weeks of age (*bottom*). Representative western blots of Ryr1 and Gapdh (*left*) $*p < .05$; $**p < .01$; $***p < .005$; $****p < .001$. Data are shown as mean $\pm$ SEM.

up to 12 weeks of age (Figure 1C). Consistent with that observed for body weight, both EDL and *soleus* muscle mass of $Ryr1^{TM/SC-\Delta L}$ mice were also significantly reduced, being ~50% that of all other genotypes at 4 weeks of age (Figure 1D, *top;* Figure S3A, *top*) and ~60%–70% of WT $RyR1^{+/+}$ and all other genotypes for the fraction of $Ryr1^{TM/SC-\Delta L}$ mice that survived up to 12 weeks of age (Figure 1D, *bottom;*Figure S3A, *bottom*).

3.2 | *Ryr1* transcript and protein expression are reduced in muscle of $Ryr1^{TM/SC-\Delta L}$ mice

While *Ryr1* transcript levels were not different in TA muscles of 4-week-old $Ryr1^{TM/SC-\Delta L}$ mice (Figure 1E, *top*), Ryr1 protein expression was reduced to only ~25% of that of WT $Ryr1^{+/+}$ mice (Figure 1F, *top*). *Ryr1* transcript (Figure 1E, *bottom*) and protein (Figure 1F, *bottom*) levels in TA muscle of 12-week-old $Ryr1^{TM/SC-\Delta L}$ mice were both reduced to ~60%

of that of age-matched WT $Ryr1^{+/+}$ mice (and the other genotypes). Reductions in the expression of both Ryr1 and the dihydropyridine receptor (Dhpr) were observed in *soleus*, FDB, *diaphragm*, and TA muscles of 12-week-old $Ryr1^{TM/SC-\Delta L}$ mice (Figure S1). Together, these results suggest a complex relationship between Ryr1 transcript and protein levels, muscle mass, and survival of $Ryr1^{TM/SC-\Delta L}$ mice during postnatal development. Interestingly, while Ryr1 expression was significantly reduced, co-immunoprecipitation studies found that Fkpb12 remained associated with Ryr1 in TA muscles of $Ryr1^{TM/SC-\Delta L}$ mice (Figure S2).

3.3 | $Ryr1^{TM/SC-\Delta L}$ mice exhibit impaired respiratory function during postnatal development

To characterize the respiratory function of $Ryr1^{TM/SC-\Delta L}$ mice during postnatal development, whole-body plethysmography was performed on all genotypes at 4, 8, and
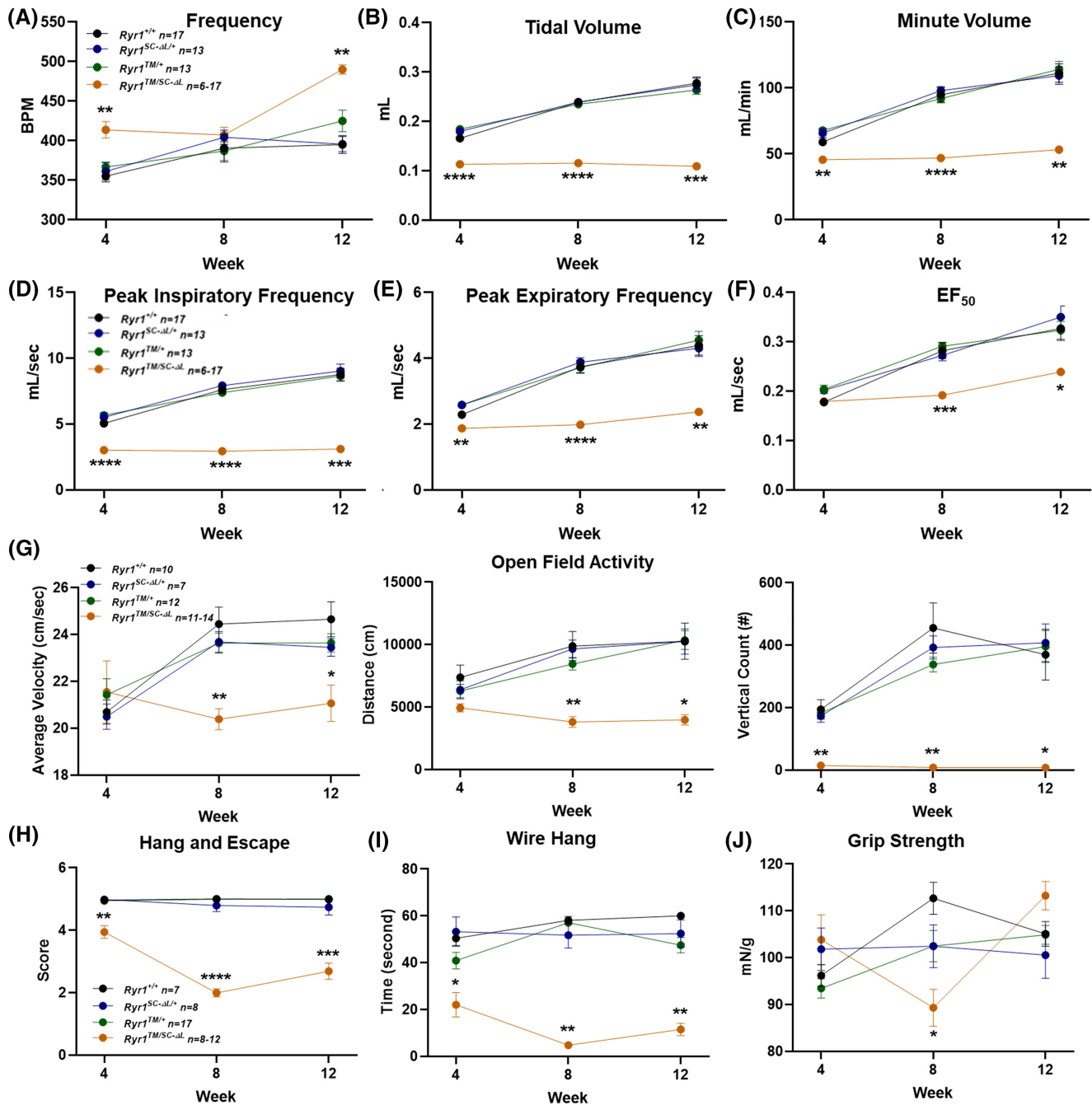
FIGURE 2 $Ryr1^{TM/SC-\Delta L}$ mice exhibit significantly reduced respiratory function and physical activity performance at 4, 8, and 12 weeks of age. $Ryr1^{TM/SC-\Delta L}$ mice exhibit significantly (A) increased breathing frequency (breaths per minute; BPM), (B) decreased tidal volume, (C) decreased minute volume, (D) decreased peak inspiratory flow, (E) decreased peak expiratory flow, and (F) decreased mid-expiratory flow (EF$_{50}$). $Ryr1^{TM/SC-\Delta L}$ mice exhibit significantly reduced locomotor activity (G), including average locomotor velocity, distance, and vertical elevation counts, as well as lower scores in hang and escape (H) and wire hang (I) tasks. Grip strength normalized to body weight was not significantly different in $Ryr1^{TM/SC-\Delta L}$ mice (J).*$p < .05$; **$p < .01$; ***$p < .005$; ****$p < .001$. Data are shown as mean ± SEM.

12 weeks of age. While not different at 8 weeks of age, breathing frequency was significantly elevated in $Ryr1^{TM/SC-\Delta L}$ mice compared to all the other genotypes at both 4 and 12 weeks of age (Figure 2A). While tidal volume, minute volume, peak inspiratory flow, peak expiratory flow, and

mid-expiratory flow (EF$_{50}$) in $Ryr1^{TM/SC-\Delta L}$ mice were largely unaltered at 4 weeks of age, all of these parameters were significantly reduced at 8 and 12 weeks of age (Figure 2B–F). Thus, $Ryr1^{TM/SC-\Delta L}$ mice exhibit progressive pulmonary dysfunction during postnatal development.

3.4 | *Ryr1^{TM/SC-ΔL}* mice exhibit reduced open-field activity and in vivo muscle strength

Given an observed apparent decrease in overall activity and movement in *Ryr1^{TM/SC-ΔL}* mice, an open-field activity assay was employed to quantitatively assess voluntary activity levels. Both average velocity (Figure 2G, *left*) and distance traveled (Figure 2G, *middle*) were significantly reduced in 8- and 12-week-old *Ryr1^{TM/SC-ΔL}* mice compared to the other genotypes, indicating a progressive reduction in locomotor activity. Notably, vertical counts, indicative of hindlimb force production, were markedly reduced in *Ryr1^{TM/SC-ΔL}* mice at all ages (Figure 2G, *right*).

Next, we performed a series of behavioral tests to assess *in vivo* muscle strength and performance. Average hang and escape scores, an indicator of core strength and motor coordination, were significantly reduced in *Ryr1^{TM/SC-ΔL}* mice across all time points (Figure 2H). Sustained grip strength, as determined by the time to fall from an inverted wire grid, was also significantly reduced in *Ryr1^{TM/SC-ΔL}* mice across all three ages tested (Figure 2I). Transient grip strength was significantly reduced in *Ryr1^{TM/SC-ΔL}* mice only at 8 weeks of age (Figure 2J). Overall, these *in vivo* behavioral results indicate that *Ryr1^{TM/SC-ΔL}* mice exhibit a significant reduction in overall activity, as well as muscle force production, performance, and motor coordination.

3.5 | *Ryr1^{TM/SC-ΔL}* mice exhibit reduced ex vivo absolute muscle force production

To assess ex vivo muscle function, isometric-specific force production in EDL muscles was measured from 3-month-old *Ryr1^{+/+}*, *Ryr1^{TM/+}*, *Ryr1^{SC-ΔL/+}*, and *Ryr1^{TM/SC-ΔL}* mice. Not surprisingly, absolute force was significantly reduced in EDL muscles from *Ryr1^{TM/SC-ΔL}* mice compared to all other genotypes (Figure 3A). However, peak specific force production (normalized to physiological CSA) was significantly reduced only for twitch stimulation (at 1 Hz stimulation), but not at higher frequencies of stimulation (Figure 3B). In addition, no shift in the relative specific force-frequency relationship was observed for EDL muscles from *Ryr1^{TM/SC-ΔL}* mice (Figure 3C). In addition, both the maximum rate of twitch force production and twitch force decline were decreased in EDL muscles from *Ryr1^{TM/SC-ΔL}* mice compared to all other genotypes (Figure 3D). Similar reductions in muscle mass, raw force production, twitch-specific force production, and a slowing in the kinetics of force production and relaxation were also observed in *soleus* muscles from 12-week-old *Ryr1^{TM/SC-ΔL}* mice (Figure S3). Interestingly, in addition to reduced raw force production and slowed kinetics of force production and relaxation, maximal specific force was reduced and the relative force-frequency relationship was right-shifted in *diaphragm* muscles from 12-week-old *Ryr1^{TM/SC-ΔL}* mice (Figure S4), findings consistent with the marked respiratory dysfunction of these mice (see Figure 2A–F).
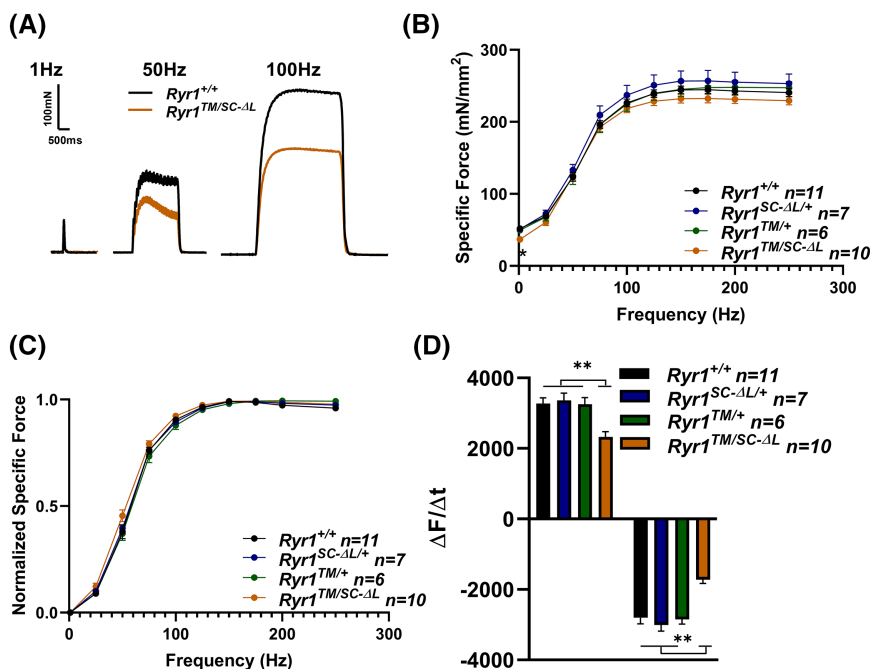
FIGURE 3 EDL muscle twitch and tetanic-specific force production in 12-week-old mice. (A) Representative superimposed traces of raw force elicited at 1 Hz (*left*), 50 Hz (*middle*), and 100 Hz (*right*) stimulation frequencies in EDL muscles from *Ryr1^{+/+}* and *Ryr1^{TM/SC-ΔL}* mice. (B and C) Absolute (B) and relative (C) specific force-frequency curves of EDL muscles for each genotype. (D) Maximum rate of peak twitch force production (*left*) and relaxation (*right*) for each genotype. *$p < .05$; **$p < .01$. Data are shown as mean ± SEM.

3.6 | $Ryr1^{TM/SC-\Delta L}$ mice exhibit reduced EDL muscle myofiber size and number

Given the reduced muscle weight and rate of contraction/relaxation in EDL muscles of $Ryr1^{TM/SC-\Delta L}$ mice, we assessed fiber type content and CSA in EDL muscles of 3-month-old $Ryr1^{+/+}$, $Ryr1^{TM/+}$, $Ryr1^{SC-\Delta L/+}$, and $Ryr1^{TM/SC-\Delta L}$ mice (Figure 4). Representative images of EDL muscle cross-sections from WT $Ryr1^{+/+}$ and $Ryr1^{TM/SC-\Delta L}$ mice are shown in Figure 4A. While EDL muscles from all four genotypes exhibited similar fiber type content (type IIb/x>IIa>I), CSA of type IIb and IIx fibers were significantly decreased, while type I fiber CSA was increased, in EDL muscles from $Ryr1^{TM/SC-\Delta L}$ mice (Figure 4B). In addition, the number of type IIB fibers (Figure 4C) and total number of muscle fibers (Figure 4D) were also significantly reduced in EDL muscles from $Ryr1^{TM/SC-\Delta L}$ mice. Similar reductions in muscle mass, type I and IIa myofiber CSA, and total number of muscle fibers were also observed in *soleus* muscles from 12-week-old $Ryr1^{TM/SC-\Delta L}$ mice (Figure S5). H&E staining revealed no increase in the percentage of central nuclei in EDL muscles from 3-month-old $Ryr1^{TM/SC-\Delta L}$ mice (Figure S6).

3.7 | FDB fibers from $Ryr1^{TM/SC-\Delta L}$ mice exhibit reduced electrically-evoked Ca^{2+} release

We assessed electrically-evoked Ca^{2+} release in single FDB fibers isolated from 4-week-old and 12-week-old $Ryr1^{+/+}$ and $Ryr1^{TM/SC-\Delta L}$ mice. For these experiments, acutely dissociated FDB fibers were loaded with mag-fluo-4, a rapid, low-affinity Ca^{2+} dye that enables temporal resolution of the magnitude and kinetics of electrically-evoked Ca^{2+} release.[23] Representative traces of relative changes in mag-fluo-4 fluorescence ($\Delta F/F_0$) during electrical twitch stimulation (Figure 5A,C) revealed a significant reduction in peak Ca^{2+} transient amplitude (1 Hz; Figure 5A,C). However, no difference was observed during high-frequency stimulation (100 Hz) in FDB fibers from either 4-week-old (Figure 5B) or 12-week-old
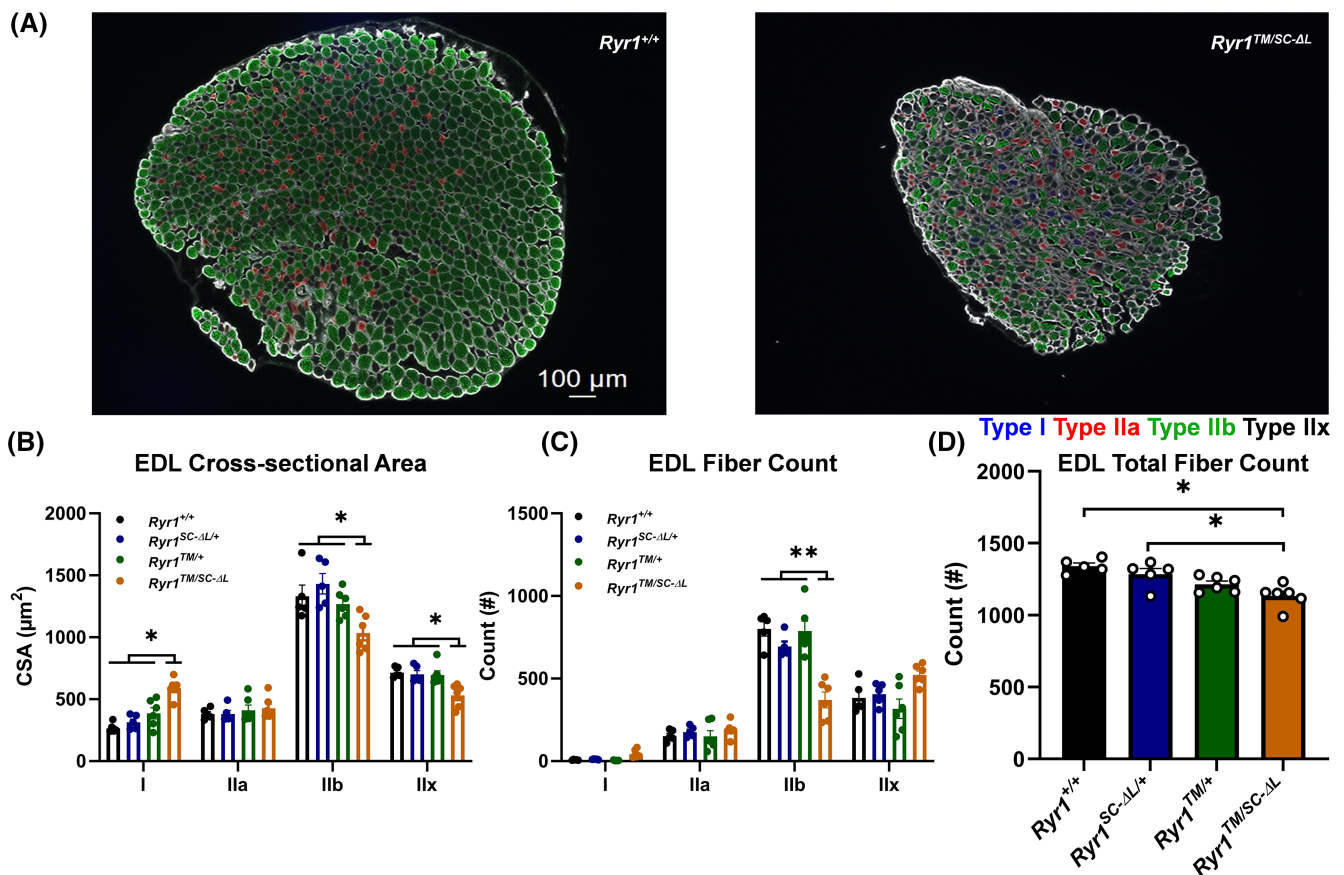
FIGURE 4 Fiber type and cross-sectional area (CSA) analyses of EDL muscles from 12-week-old mice. (A) Representative fiber-type staining images of EDL muscle sections from $Ryr1^{+/+}$ (*left*) and $Ryr1^{TM/SC-\Delta L}$ (*right*) mice. The scale bar shown in panel A (100 μm) applies to both images. (B) CSA, (C) fiber type fiber count, and (D) total fiber count in EDL muscles for each genotype. *$p < .05$; **$p < .01$. Data are shown as mean ± SEM.

FIGURE 5 Electrically evoked twitch and tetanic Ca^{2+} transients in FDB fibers from $Ryr1^{+/+}$ and $Ryr1^{TM/SC-\Delta L}$ mice. (A, B) Representative superimposed traces (*left*) and peak change in relative mag-fluo-4 fluorescence (*right*) elicited during electrically-evoked tw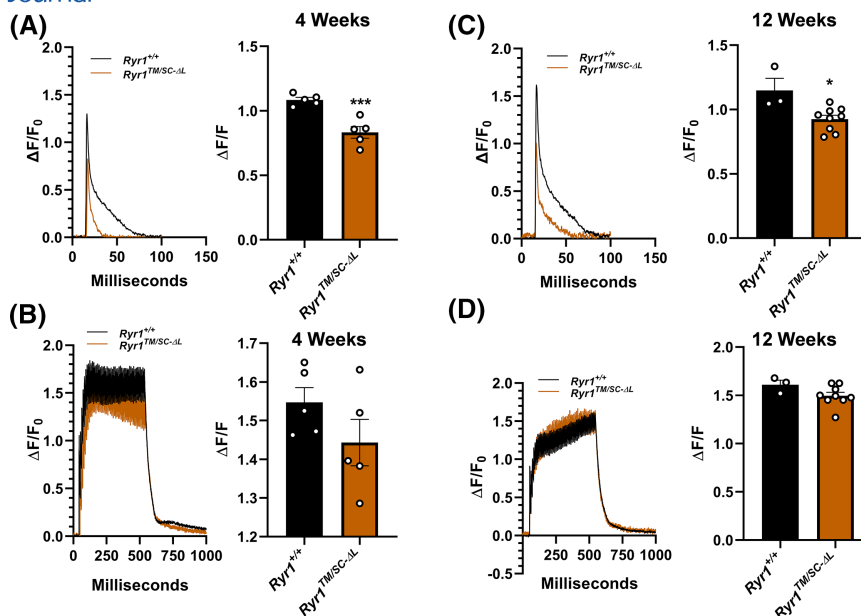itch (A) and 100 Hz (B) stimulation in FDB fibers from 4-week-old $Ryr1^{+/+}$ and $Ryr1^{TM/SC-\Delta L}$ mice. (C, D). Representative superimposed traces (*left*) and peak change in relative mag-fluo-4 fluorescence (*right*) elicited during electrically-evoked twitch (A) and 100 Hz (B) stimulation in FDB fibers from 12-week-old $Ryr1^{+/+}$ and $Ryr1^{TM/SC-\Delta L}$ mice. *$p < .05$; ***$p < .005$. Data are shown as mean ± SEM.

(Figure 5D) $Ryr1^{TM/SC-\Delta L}$ mice compared to that observed for age-matched $Ryr1^{+/+}$ mice. To further assess potential effects on the rate of Ca^{2+} release and reuptake, we compared the kinetics of electrically evoked twitch Ca^{2+} transients in FDB fibers from 4-week (Figure S7) and 12-week (Figure S8) old mice. For these analyses, the decay phase of the transient was fit to a double exponential equation where the fast component of decay primarily reflects Ca^{2+} binding to fast myoplasmic Ca^{2+} buffers (A_{fast} and τ_{fast}), and the slow component of decay is dominated by SERCA-dependent Ca^{2+} reuptake (A_{slow} and τ_{slow}).[22,23] Representative, normalized mag-fluo-4 traces and corresponding double exponential fits are shown for FDB fibers from 4-week-old $Ryr1^{+/+}$ and $Ryr1^{TM/SC-\Delta L}$ mice in Figure S7A. The reduction in Ca^{2+} transient integral observed in FDB fibers from $Ryr1^{TM/SC-\Delta L}$ mice (Figure S7D) reflected a similar reduction in both A_{fast} and A_{slow} (Figure S7E,F) without a change in corresponding time constants (Figure S7B,C). In addition, the maximum rate of increase in the electrically-evoked mag-fluo-4 fluorescence, an estimate of Ca^{2+} release flux, was significantly reduced in FDB fibers from 4-week-old $Ryr1^{TM/SC-\Delta L}$ mice (Figure S7G). A similar reduction in Ca^{2+} transient integral (Figure S8D), A_{fast} (Figure S8E) but not A_{slow} (Figure S8F), and the maximum rate of increased mag-fluo-4 fluorescence (Figure S8G) was also observed in FDB fibers from 12-week-old $Ryr1^{TM/SC-\Delta L}$ mice. The results in Figures S7G and S8G indicate that peak Ca^{2+} release flux is reduced in FDB fibers from 4-week and 12-week-old $Ryr1^{TM/SC-\Delta L}$

mice, consistent with the significant reduction in Ryr1 protein expression observed at both ages (Figure 1F).

3.8 | $Ryr1^{TM/SC-\Delta L}$ mice exhibit RYR1 channels with increased Ca^{2+} leak

Given that prior studies reported that the Ryr1 mutations engineered into $Ryr1^{TM/SC-\Delta L}$ mice result in increased RYR1 channel open probability at low cytosolic Ca^{2+} concentrations, we compared the rate of SR Ca^{2+} leak in FDB fibers from 4-week-old (Figure 6A,C) and 12-week-old (Figure 6B,D) WT $Ryr1^{+/+}$ and $Ryr1^{TM/SC-\Delta L}$ mice. For these experiments, single FDB fibers loaded with fura-2 were used to quantify the resting free Ca^{2+} concentration (Figure 6E). Subsequent blockage of SERCA pumps by addition of 30 µM cyclopiazonic acid (CPA) in a Ca^{2+}-free Ringer's solution results in a gradual rise in resting Ca^{2+} that is proportional to the rate of SR Ca^{2+} leak (see Figure 6A,B), which is dominated by steady-state Ca^{2+} flux through RYR1 Ca^{2+} release channels.[25] Interestingly, the maximum rate of SR Ca^{2+} leak in FDB from $Ryr1^{+/+}$ and $Ryr1^{TM/SC-\Delta L}$ mice was not significantly different at either 4 weeks (Figure 6C) or 12 weeks (Figure 6D) of age. However, the maximum rate of SR Ca^{2+} leak was two- to threefold greater at 4 weeks of age compared to that observed at 12 weeks of age for both genotypes (compare Figure 6C,D). However, Ryr1 expression in FDB muscles is reduced ~70% at 4 and 12 weeks of age (see Figure S1B, *top*).
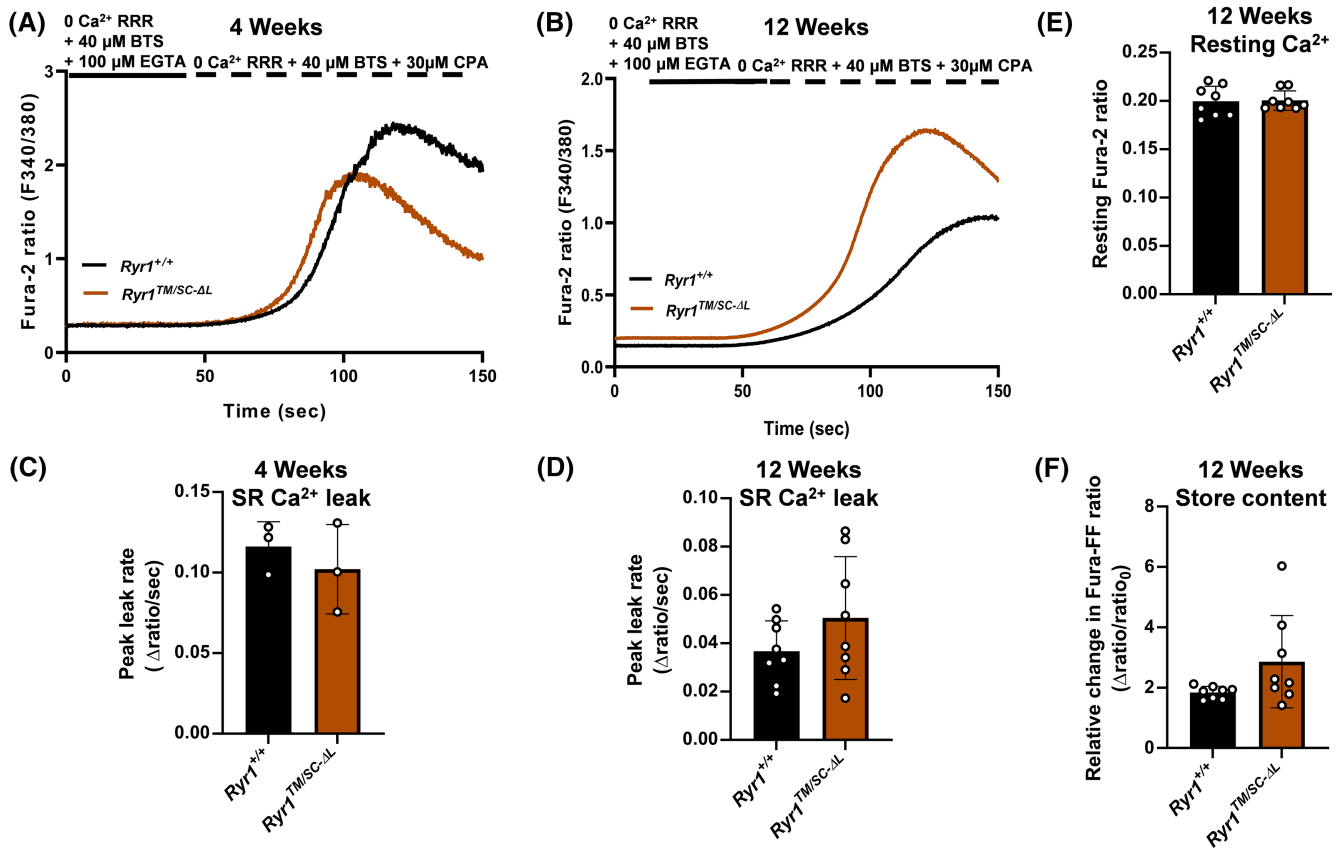
FIGURE 6 Ryr1 Ca^{2+} leak, resting Ca^{2+}, and Ca^{2+} store content measurements in FDB fibers from 4 and 12 weeks of age. (A, B) Representative fura-2 traces during the application of 30 μM cyclopiazonic acid (CPA), SERCA pump inhibitor, in FDB fibers from 4-week-old (A) and 12-week-old (B) $Ryr1^{+/+}$ and $Ryr1^{TM/SC-\Delta L}$ mice. (C, D) Peak Ryr1 Ca^{2+} leak rate of fura-2 loaded FDB fibers during CPA application. (E) Resting fura-2 ratio in FDB fibers from 12-week-old $Ryr1^{+/+}$ and $Ryr1^{TM/SC-\Delta L}$ mice. (F) Total releasable Ca^{2+} store content in fura-FF-loaded FDB fibers from 12-week-old $Ryr1^{+/+}$ and $Ryr1^{TM/SC-\Delta L}$ mice. Data are shown as mean ± SEM.

Thus, assuming the SR Ca^{2+} leak is entirely via RYR1 channels, the rate of RYR1 Ca^{2+} leak per channel is ~threefold higher in FDB fibers from $Ryr1^{TM/SC-\Delta L}$ mice. Neither resting free Ca^{2+} concentration (Figure 6E) nor total Ca^{2+} store content (Figure 6F) were significantly different between FDB fibers from 12-week-old $Ryr1^{+/+}$ and $Ryr1^{TM/SC-\Delta L}$ mice, consistent with the similar net rate of SR Ca^{2+} leak observed under these conditions. Overall, our results indicate that increased RYR1 Ca^{2+} leak/channel is the major RYR1 functional defect in the muscle of $Ryr1^{TM/SC-\Delta L}$ mice, and moreover, that a reduction in RYR1 protein expression may represent a protective adaptation of muscle designed to mitigate this effect.

3.9 | Proteomic analyses of skeletal muscle from $Ryr1^{TM/SC-\Delta L}$ mice

To comprehensively assess changes in the skeletal muscle proteome of $Ryr1^{TM/SC-\Delta L}$ mice, we performed mass spectrometry analyses of *gastrocnemius* muscles from 4 and 12-week-old male $Ryr1^{+/+}$ and $Ryr1^{TM/SC-\Delta L}$ mice (n = 4

each). From >3500 proteins identified by mass spectrometry, a total of 515 (Table 1) and 315 proteins (Table 2) were significantly altered in muscle of $Ryr1^{TM/SC-\Delta L}$ mice compared to that of $Ryr1^{+/+}$ mice at 4 weeks and 12 weeks of age, respectively (Figure 7A). More specifically, 140 proteins were significantly increased and 375 proteins were significantly decreased in muscle of $Ryr1^{TM/SC-\Delta L}$ mice at 4 weeks of age, while 145 proteins were increased and 170 proteins were decreased at 12 weeks (Figure 7A, donut charts). Cellular Component Enrichment Go Pathway analyses of the 375 significantly decreased proteins at 4 weeks of age revealed alterations in aminoacyl-tRNA synthetases, translation initiation and preinitiation factors, ribosomal subunits, and chaperone-containing T-complex proteins. The dystroglycan/sarcoglycan/dystrophin-associated glycoprotein (DAG) complexes, lamin filaments, nuclear lamina, and (auto)lysosomes were among the major altered pathways observed for the 140 proteins found to be increased in muscle from $Ryr1^{TM/SC-\Delta L}$ mice (Figure 7B, *left*). Parallel Cellular Component Enrichment Go Pathway analyses found the fibrinogen complex, aminoacyl-tRNA synthetases, and chaperone complexes to be among the

TABLE 1 List of significantly altered proteins in muscle of 4-week-old $Ryr1^{TM/SC-\Delta L}$ mice.

Proteins	Fold change (Log$_2$) at 4 weeks
*Serpina3k	−1.29
Bdh1	−1.01
Usp13	−0.90
Rab3a	−0.76
Tfrc	−0.68
Klhl31	−0.67
Afm	−0.66
Prkar1a	−0.63
Ryr1;Ryr2	−0.63
Tars3	−0.62
Ryr1	−0.59
Ahsg	−0.55
Myo18b	−0.54
Mrps5	−0.51
Map2k6	−0.51
Serpinh1	−0.50
Actg2	−0.50
Suclg2	−0.49
Gc	−0.49
Aimp2	−0.47
Carm1	−0.46
Nexn	−0.46
Mars1	−0.44
Phkb	−0.44
Aimp1	−0.44
Msrb3	−0.43
Eprs1	−0.43
Iars1	−0.40
Tf	−0.40
Nek9	−0.40
Pfkm	−0.40
Chmp4b	−0.40
Arf2;Arf4;Arf5	−0.40
Colgalt1	−0.40
Hpx	−0.40
Mat2a	−0.40
Fxr1	−0.39
Palld	−0.39
Phka1	−0.38
Dnajc7	−0.38
Phkg1	−0.38
Pygm	−0.38

TABLE 1 (Continued)

Proteins	Fold change (Log$_2$) at 4 weeks
Serping1	−0.37
Txlnb	−0.37
Rpl27a	−0.37
Srp72	−0.37
Dars1	−0.37
Rcsd1	−0.36
Slc37a4	−0.36
Sar1b	−0.35
Edf1	−0.35
Hdlbp	−0.35
Eps15	−0.35
Rpl12	−0.35
Clic5	−0.35
Rpl3l	−0.35
C3	−0.35
Fkbp4	−0.35
Gphn	−0.34
Map2k2	−0.34
Cluh	−0.34
Rpl13a	−0.34
Rab18	−0.34
Pgam1;Pgam2	−0.33
Rpl6	−0.33
Agl	−0.33
Rpl14	−0.33
Mesd	−0.33
Oxct1	−0.33
Rab7a	−0.33
Ldha	−0.32
Rps11	−0.32
Kars1	−0.32
Rrbp1	−0.32
Rpl5	−0.32
Rps4x	−0.32
Nt5c1a	−0.31
Rpl13	−0.31
Rpl8	−0.31
Tmx2	−0.31
Pygb;Pygl;Pygm	−0.31
Eif4a2	−0.31
Srp68	−0.31
Pkm	−0.31
Caprin1	−0.30

TABLE 1 (Continued)

Proteins	Fold change (Log$_2$) at 4 weeks
Rab12	−0.30
Tmod1	−0.30
Ubap2	−0.30
Rpl19	−0.30
Rplp0	−0.30
Lars1	−0.30
Qars1	−0.30
Cct4	−0.30
Rps18	−0.30
Eif5b	−0.30
Metap2	−0.29
Fam98a	−0.29
Gls	−0.29
Rps12	−0.29
Rps2	−0.29
Rpl27	−0.29
Rps25	−0.29
Rpl23a	−0.29
Cct5	−0.29
Ndufaf1	−0.28
Rps3a	−0.28
Prkaa2	−0.28
Rpl26	−0.28
Eef2	−0.28
Rps10	−0.28
Rars1	−0.28
Cct6a	−0.28
Tcp1	−0.28
Rpl11	−0.28
Rab1A	−0.28
Pon3	−0.28
Slc25a4;Slc25a5	−0.28
Nme1;Nme2	−0.28
Cct8	−0.28
Sqor	−0.28
Naca	−0.28
Rpl10	−0.28
Creld1	−0.28
Rpl7a	−0.28
Fhod1	−0.27
Rpl9	−0.27
Cct3	−0.27
Srp54	−0.27

(Continues)

TABLE 1 (Continued)

Proteins	Fold change (Log$_2$) at 4 weeks
Rpl30	−0.27
Cct2	−0.27
Tars1	−0.27
Rpl24	−0.27
Map2k3	−0.27
Rab1b	−0.27
Cand2	−0.27
Impdh2	−0.27
Rpl35a	−0.27
Rps20	−0.26
Serbp1	−0.26
Rpl15	−0.26
Gcn1	−0.26
Ide	−0.26
Rps17	−0.26
Carnmt1	−0.26
Acsl6	−0.26
Rpl17	−0.26
Lrpprc	−0.26
Rpl7	−0.26
Rpl31	−0.26
Idh3b	−0.26
Ctps1	−0.26
Mat2b	−0.26
Idh3a	−0.26
Rpsa	−0.26
Atp2a1;Atp2a3	−0.26
Rps13	−0.26
Abcf2	−0.25
Ndufb10	−0.25
Trim54	−0.25
Hsp90b1	−0.25
Rps9	−0.25
Usp47	−0.25
Myo18a	−0.25
Suclg1	−0.25
Dusp3	−0.25
Tmed7	−0.25
Suox	−0.25
Ica	−0.25
Arcn1	−0.25
Upf1	−0.25
Arih1	−0.25

(Continues)

The FASEB Journal

TABLE 1 (Continued)

Proteins	Fold change (Log$_2$) at 4 weeks
Cct7	−0.24
Lrpap1	−0.24
Kif1b	−0.24
Fam114a2	−0.24
Tpp2	−0.24
Farsa	−0.24
Rack1	−0.24
Lmod3	−0.24
Eif3f	−0.24
Hook3	−0.24
Ogt	−0.24
Gyg1	−0.24
Rpl37a	−0.24
Eif3m	−0.24
Eef1g	−0.24
Flii	−0.24
Eif2a	−0.24
Gbe1	−0.23
Rpl10a	−0.23
Emc3	−0.23
Ugp2	−0.23
Sec22b	−0.23
Usp24	−0.23
Sod2	−0.23
Synm	−0.23
Tmem109	−0.23
Cacnb1	−0.23
Rps15a	−0.23
Eif2s2	−0.23
Rpl18a	−0.23
Gart	−0.23
Sec31a	−0.23
Farsb	−0.23
Rps8	−0.23
Mapkapk2	−0.23
Rabggta	−0.23
Rps19	−0.23
Rps7	−0.23
Homer1	−0.23
Ppp1r3a	−0.22
Eif3g	−0.22
Rpn2	−0.22
Eif2s3x;Eif2s3y	−0.22

TABLE 1 (Continued)

Proteins	Fold change (Log$_2$) at 4 weeks
Sec23ip	−0.22
Tmx3	−0.22
Cpox	−0.22
Prkab2	−0.22
Rps6	−0.22
Rps5	−0.22
Bag2	−0.22
Lman1	−0.22
Rps3	−0.22
Gpi	−0.22
Ndrg2	−0.22
Cacna1s	−0.22
Idh3g	−0.21
Copg1	−0.21
Maoa	−0.21
Ybx1	−0.21
Tst	−0.21
Glg1	−0.21
Arfgap2	−0.21
Rps14	−0.21
Rab21	−0.21
Ppp6c	−0.21
Calr	−0.21
Pcyt2	−0.21
Rpl23	−0.20
Erap1	−0.20
Cops7a	−0.20
Samhd1	−0.20
Ckap5	−0.20
Usp4	−0.20
Sec13	−0.20
Dync1i2	−0.20
Eef1d	−0.20
Clasp1	−0.20
Clip1	−0.20
Csde1	−0.20
Dnajb11	−0.20
Eif3b	−0.20
Pabpc1	−0.20
Etf1	−0.19
Abhd16a	−0.19
Mdh2	−0.19
Eif4a1;Eif4a2	−0.19

TABLE 1 (Continued)

Proteins	Fold change (Log$_2$) at 4 weeks
Ubap2l	−0.19
Apeh	−0.19
Eif3c	−0.19
Nudc	−0.19
Eef1a2	−0.19
Eif3d	−0.19
Spr	−0.19
Chordc1	−0.19
Rab10	−0.19
Ubr4	−0.19
Abcf3	−0.18
Opa1	−0.18
Actr10	−0.18
Eif3l	−0.18
Fn1	−0.18
Fyco1	−0.18
Ipo7	−0.18
Eif3i	−0.18
Gpx4	−0.18
Oat	−0.18
Eif3a	−0.18
Nqo2	−0.18
Trim72	−0.18
Ykt6	−0.17
Ak3	−0.17
Cops6	−0.17
Psme2	−0.17
Anxa3	−0.17
Stt3b	−0.17
Rpn1	−0.17
Stt3a	−0.17
Ethe1	−0.17
Eif2s1	−0.17
Dst	−0.17
Rab2a	−0.17
Tmed2	−0.17
Vdac1	−0.17
Gps1	−0.16
Mapk14	−0.16
Lman2	−0.16
Rpl32	−0.16
Usp15	−0.16
Pabpc4	−0.16

(Continues)

TABLE 1 (Continued)

Proteins	Fold change (Log$_2$) at 4 weeks
Glrx3	−0.16
Strn3	−0.16
Eif4g2	−0.16
Ddx3x;Ddx3y	−0.16
Plin3	−0.16
Rps23	−0.16
Rheb	−0.16
Eif3e	−0.16
Ddost	−0.16
Pcbp2	−0.16
Calu	−0.16
Pa2g4	−0.15
Actr1a	−0.15
Eif4g1	−0.15
Cops2	−0.15
Cops4	−0.15
Dnm1l	−0.15
Mybbp1a	−0.15
Eif1ax	−0.15
Uchl5	−0.15
Dnaja2	−0.15
Rab11b	−0.15
Atl2	−0.15
Ncln	−0.15
Gspt1;Gspt2	−0.14
Actr1a;Actr1b	−0.14
Eef1b	−0.14
Cul3	−0.14
Unc45b	−0.14
Naa15	−0.14
Eef1a1;Eef1a2	−0.14
Cars1	−0.14
Cisd1	−0.14
Txnrd1	−0.14
Prkcsh	−0.14
Cops5	−0.14
Ktn1	−0.13
Shmt2	−0.13
Ccdc47	−0.13
Eif3j1;Eif3j2	−0.13
Slc41a3	−0.13
Rab6a	−0.13
Ppp6r3	−0.13

(Continues)

TABLE 1 (Continued)

Proteins	Fold change (Log$_2$) at 4 weeks
P4hb	−0.13
Kpna1	−0.13
Hbs1l	−0.13
Psma6	−0.13
Erp44	−0.13
Hyou1	−0.13
Stip1	−0.12
Hectd1	−0.12
Ufl1	−0.12
Dctn1	−0.12
Ppp5c	−0.11
Sacm1l	−0.11
Dync1li1	−0.11
Emc2	−0.11
Cul2	−0.11
Psma2	−0.11
Psmd1	−0.11
Sars1	−0.11
Sec24c	−0.11
Mpi	−0.10
Dlg1	−0.10
Dnpep	−0.09
Rab14	−0.09
Usp9x	−0.09
Isoc1	−0.09
Ppp2r2a	−0.09
Trap1	−0.09
Ddx6	−0.09
Psmb5	−0.09
Lnpk	−0.08
Psmc5	−0.07
Get3	−0.06
Cdh13	0.06
Fermt2	0.08
Wdr1	0.09
Ehd1	0.09
Limch1	0.09
Hnrnph1;Hnrnph2	0.10
Cavin1	0.10
Prkaca	0.10
Atp6v1a	0.10
Twf2	0.10
Nono	0.11

TABLE 1 (Continued)

Proteins	Fold change (Log$_2$) at 4 weeks
*Sgca	0.12
Tln1	0.12
Apex1	0.12
Itgb1	0.12
Alpk3	0.13
Srsf1	0.13
Snrnp200	0.13
Gsr	0.13
Alyref	0.14
Srsf7	0.14
Dbt	0.14
Tomm40	0.14
Camk2d	0.14
Fus	0.14
Stxbp3	0.14
Nop56	0.14
Prpf8	0.14
*Dmd	0.15
Por	0.15
Dhx9	0.15
Eftud2	0.15
Col4a1	0.15
Tom1	0.15
Lemd2	0.15
Lamp1	0.15
Ddx39b	0.15
Prkar2a	0.15
Trip10	0.16
Map3k20	0.16
Nae1	0.16
Hnrnpm	0.17
Hnrnpu	0.17
Acad8	0.17
Gstz1	0.17
Sgcd	0.17
Myo1c	0.18
Cyb5r3	0.18
Esyt1	0.18
Cutc	0.19
Trim28	0.19
Itga7	0.19
Gcdh	0.19
Sgcg	0.19

TABLE 1   (Continued)

Proteins	Fold change (Log$_2$) at 4 weeks
Matr3	0.19
Khsrp	0.19
Akr1e2	0.19
Hspb8	0.20
Rps27a;Uba52	0.20
Tmpo	0.20
Adipoq	0.20
Anxa4	0.20
Prpf19	0.20
Ilk	0.21
Abra	0.21
Fbl	0.21
Lbr	0.21
Dag1	0.21
Hnrnpl	0.22
Lmnb2	0.22
Hmgb1	0.23
Cenpv	0.24
Tpr	0.24
Ghitm	0.24
Bcap29	0.24
Pacsin3	0.24
Ctsb	0.25
Hnrnpd	0.25
Lamp2	0.25
Thrap3	0.25
Camk2b	0.26
Flot2	0.26
Snrpb;Snrpn	0.26
Fabp4	0.26
Pdcd6	0.27
Prune1	0.27
Septin11	0.27
Nup93	0.27
Ablim2	0.28
Lmna	0.28
Sgcb	0.29
Slc12a2	0.29
Bcat2	0.29
Emd	0.29
Tor1aip1	0.30
Cmas	0.30
Scp2	0.30

(Continues)

TABLE 1   (Continued)

Proteins	Fold change (Log$_2$) at 4 weeks
Ctsd	0.30
Flot1	0.30
Ppp2r5a	0.30
Aldh2	0.30
Myl6	0.32
Adhfe1	0.32
H4f16	0.32
Adh1	0.32
Ca3	0.32
Tkt	0.32
*Acly	0.33
Sun1	0.34
Selenbp1	0.35
Actn1	0.36
Nxn	0.36
Lmnb1	0.37
Mecp2	0.37
Anpep	0.38
Mylk	0.38
Gaa	0.38
Sorbs1	0.39
H1-0	0.42
Gpx3	0.42
Skp1	0.45
Hp1bp3	0.47
*Fasn	0.47
Acox1	0.48
Fbln5	0.49
Akt2	0.50
Fth1	0.53
Uqcrh	0.54
Ablim1	0.59
Postn	0.59
Sorbs2	0.61
Aoc3	0.63
Slmap	0.69
Uchl1	0.77
Mcpt4	0.85
Nefh	1.06
Plin1	1.07
Nefl	1.10
Ces1d	1.25
Glul	1.38

*Proteins changes tested by western blot in Figure S6.

TABLE 2 List of significantly altered proteins in muscle of 12-week-old $Ryr1^{TM/SC-\Delta L}$ mice.

Proteins	Fold Change (Log$_2$) at 12 weeks
Fga	−2.02
Fgb	−2.02
Ighm	−1.96
Cfh	−1.91
Fgg	−1.88
Mug1	−1.77
Afm	−1.70
Pzp	−1.67
*Serpina3k	−1.60
Apoe	−1.44
C3	−1.33
Hpx	−1.28
Gc	−1.27
Hrg	−1.27
Apoa1	−1.27
Plg	−1.27
Itih4	−1.24
Spta1	−1.24
Apoh	−1.22
Slc4a1	−1.20
Serpinf2	−1.18
Cp	−1.17
Ces1c	−1.15
Cfb	−1.12
Kng1	−1.12
Thbs1	−0.97
Fn1	−0.96
Ica	−0.90
Ahsg	−0.90
Tf	−0.87
Ppid	−0.86
Itih2	−0.86
Serping1	−0.82
F2	−0.79
Serpinc1	−0.77
Hsph1	−0.76
Tmx2	−0.73
Alb	−0.70
Oplah	−0.65
Ank1	−0.64
Blvrb	−0.64
Tars3	−0.63
Serpinh1	−0.62

TABLE 2 (Continued)

Proteins	Fold Change (Log$_2$) at 12 weeks
Sqor	−0.60
Nt5c1a	−0.52
Slc41a3	−0.51
Fubp1	−0.51
Dars1	−0.51
Fkbp4	−0.50
Carnmt1	−0.47
Eprs1	−0.47
Glg1	−0.47
Aimp2	−0.46
Aimp1	−0.45
Trip12	−0.44
Map2k6	−0.44
Apeh	−0.44
St13	−0.43
Rnpep	−0.43
Lcp1	−0.43
Cand2	−0.40
Hsp90aa1	−0.38
Mars1	−0.38
Mmab	−0.38
Fdps	−0.38
Ogt	−0.36
Bag2	−0.36
Edf1	−0.35
Fkbp3	−0.35
Eps15	−0.34
Rars1	−0.34
Rab3a	−0.34
Stip1	−0.34
Cdc37	−0.34
Hspbp1	−0.33
Blmh	−0.32
Bcs1l	−0.31
Usp24	−0.31
Cul3	−0.31
Kars1	−0.31
Cct8	−0.30
Iars1	−0.30
Srp68	−0.29
Hsp90b1	−0.29
Farsb	−0.29
Prkab2	−0.28
Tmem109	−0.28

TABLE 2 (Continued)

Proteins	Fold Change (Log$_2$) at 12 weeks
Qars1	−0.28
Cct2	−0.27
Czib	−0.27
Ryr1	−0.27
Nqo2	−0.26
Srp72	−0.26
Fundc2	−0.26
Cct4	−0.26
Ryr1;Ryr2	−0.26
Cct5	−0.26
Hagh	−0.26
Sec31a	−0.26
Nudt2	−0.25
Pdxk	−0.25
Gsn	−0.25
Cct7	−0.25
Farsa	−0.25
Hsp90ab1	−0.24
Cdv3	−0.24
Clasp1	−0.24
Pank4	−0.24
Hdhd2	−0.23
Abhd16a	−0.23
Fam98a	−0.23
Cct6a	−0.23
Hsp90aa1;Hsp90ab1	−0.23
Srp54	−0.23
Prkaa2	−0.23
Cct3	−0.22
Asph	−0.22
Myorg	−0.22
Tcp1	−0.22
Isoc1	−0.22
Bpnt1	−0.22
Mlf1	−0.22
Npepl1	−0.22
Hspa2;Hspa8	−0.21
Calr	−0.21
Hspa8	−0.21
Ahsa1	−0.20
Nme2	−0.20
Macrod1	−0.20
Rpn1	−0.20
Lman1	−0.20

(Continues)

TABLE 2 (Continued)

Proteins	Fold Change (Log$_2$) at 12 weeks
Naa25	−0.20
Lars1	−0.20
Glod4	−0.19
Akr7a2	−0.19
Arpc3	−0.19
Grb2	−0.19
Ppp5c	−0.19
Pdia3	−0.19
Jph2	−0.19
Cul4a	−0.18
Prdx1	−0.18
Kpna3	−0.18
Eef1a1;Eef1a2	−0.17
Eif3d	−0.17
Hdlbp	−0.16
Hhatl	−0.16
Txnrd1	−0.16
Snx5	−0.16
Prps1	−0.16
Tbcb	−0.16
Gart	−0.16
Eef1a2	−0.16
Glo1	−0.14
Ap2a1;Ap2a2	−0.14
Oat	−0.14
Abcf1	−0.14
Rpn2	−0.14
Plaa	−0.14
Gyg1	−0.13
Memo1	−0.12
Eef1g	−0.12
Pa2g4	−0.12
Ppp1r3a	−0.11
Hook3	−0.11
Cul2	−0.11
Blvra	−0.10
Eif3e	−0.08
Synpo2l	−0.07
Ppa1	−0.06
Syncrip	0.07
Dync1h1	0.08
Vapa	0.09
Gars1	0.09
Rpl31	0.10

(Continues)

T A B L E 2 (Continued)

Proteins	Fold Change (Log$_2$) at 12 weeks
Actr1a;Actr1b	0.10
Rsu1	0.10
Rpl27a	0.12
Prep	0.12
Bcap31	0.12
Mypn	0.12
Wars1	0.13
Adss1	0.13
Pdcd5	0.14
Capza1	0.14
Otub1	0.15
Gpd1l	0.15
Qdpr	0.15
Lrrc47	0.15
Rps20	0.15
Ncl	0.16
Sypl2	0.16
Ufd1	0.16
Mapk12	0.16
Gdi1;Gdi2	0.17
Arhgdia	0.17
Rps23	0.17
Mpst	0.17
Prmt1	0.17
Map2k3	0.17
Rab7a	0.18
Gstm5	0.18
Aamdc	0.18
Tln2	0.18
Hspb2	0.20
Speg	0.20
Dcaf6	0.20
Comt	0.20
Col4a1	0.20
Mapk1;Mapk3	0.20
G3bp2	0.21
Fbl	0.21
Lcmt1	0.21
*Sgca	0.21
Rab2a	0.22
Dtna	0.22
Alkbh3	0.22
Rps6kb2	0.22
Snrpb;Snrpn	0.22

T A B L E 2 (Continued)

Proteins	Fold Change (Log$_2$) at 12 weeks
Dpp3	0.22
Snta1	0.22
Hspb3	0.23
Cdh13	0.24
Ahcy	0.24
Hnrnpab	0.24
Cobl	0.24
Nae1	0.25
Phospho1	0.25
Impdh2	0.25
Plin4	0.25
Jph1	0.25
Eif4a1	0.25
Anxa11	0.26
Mylk2	0.26
Huwe1	0.26
Nid1	0.27
Colgalt1	0.27
Hnrnpa3	0.27
Col4a2	0.27
Tceal5	0.27
Psmd14	0.27
Lmnb1	0.27
Sgcg	0.27
Hdgf	0.27
Srl	0.27
Lama2	0.28
*Dmd	0.28
Pfn1	0.28
Acsl6	0.28
Bcap29	0.29
Lamc1	0.29
Tpt1	0.29
Sgcb	0.29
Nid2	0.30
Ppp3ca;Ppp3cb	0.30
Mapk1	0.30
Ddx5	0.30
Sgcd	0.30
Nploc4	0.30
Lamb1	0.31
Lpp	0.32
Txnl1	0.32
Eif4a3	0.33

TABLE 2 (Continued)

Proteins	Fold Change (Log$_2$) at 12 weeks
Nt5c3a	0.33
Ddx17;Ddx5	0.33
Phykpl	0.33
Flot2	0.34
Dag1	0.35
Col15a1	0.35
Klhl40	0.35
Pacsin3	0.36
Acaca;Acacb	0.37
Lmnb2	0.37
Cmas	0.37
Flot1	0.38
Herc4	0.38
Akr1a1	0.39
Camk2d	0.40
Slc3a2	0.40
Pdlim3	0.40
Aarsd1	0.40
Glul	0.40
Eef1a1	0.40
Art3	0.41
Gfus	0.42
Eif4g3	0.43
Alg2	0.44
Ranbp2	0.45
Rps6ka3	0.46
Sae1	0.46
Bsg	0.47
Xpnpep1	0.49
Tmem43	0.49
Ybx3	0.49
Dysf	0.50
Gpt2	0.51
Sms	0.51
Sorbs2	0.51
Ppp3cb	0.52
Rab18	0.53
Slc16a3	0.55
Anxa4	0.55
Skp1	0.59
Uqcrh	0.60
Fth1	0.61
Fkbp5	0.61
Tsn	0.74

(Continues)

TABLE 2 (Continued)

Proteins	Fold Change (Log$_2$) at 12 weeks
Pm20d2	0.75
*Col3a1	0.92
Uchl1	0.98
Smyd2	0.98
Cnp	1.00
Rbm3	1.17
*Acly	1.61
*Fasn	2.05

*Proteins changes tested by western blot in Figure S6.

most altered pathways for the 170 significantly decreased proteins in muscle from 12-week-old $Ryr1^{TM/SC-\Delta L}$ mice, with the dystroglycan, sarcoglycan, DAG, and calcineurin complexes among the top altered pathways identified for the 145 significantly increased proteins identified at 12 weeks of age (Figure 7B, *right*).

The proteomic analyses identified 124 common proteins (96 decreased and 28 increased) that were significantly altered in the muscle of 4-week and 12-week-old $Ryr1^{TM/SC-\Delta L}$ mice (Figure 7B, *middle*; Table 3). Consistent with the western blot results shown in Figure 1F, the proteomic analyses confirmed that Ryr1 protein expression was significantly reduced at both 4 weeks and 12 weeks, with the fold-reduction being greater at 4 weeks (Table 3). In addition to Ryr1, other specific proteins significantly decreased in the muscle of both 4 and 12-week-old $Ryr1^{TM/SC-\Delta L}$ mice were consistent with reduced tRNA aminoacylation (Tars3, Aimp1, Aimp2, Mars, Eprs1, and Lars1), protein chaperones (Bag2, Calr, Sec31a, and Hsp90b1), and serine protease inhibitors (Serpina1a, Serpina1c, Serpina1d, Serpina1e, Serpina3k, Serpina3m, Serpinh1, and Serping1) (Table 3). On the other hand, proteins involved in mitochondrial function/fatty acid metabolism (Fasn, Glul, Uqcrh, Fth1, and Acly), protein ubiquitination/degradation (Uchl1, Skp1), and skeletal muscle membrane stability (Dmd, Dag, Sgca, Sgcb, Sgcd, and Sgcg) (Table 3) were all significantly increased in muscle of 4 and 12-week-old $Ryr1^{TM/SC-\Delta L}$ mice. Importantly, quantitative western blot analyses of *gastrocnemius* muscles from both 4- and 12-week-old $Ryr1^{TM/SC-\Delta L}$ mice confirmed significant upregulation of dystrophin (Dmd), sarcoglycan alpha (Sgca), fatty acid synthase (Fasn), ATP citrate lyase (Acly), and collagen type 3 alpha 1 chain (Col3a1), though not a reduction in serine peptidase inhibitor A3K (Serpina3k) (Figure S9). Cellular Component Enrichment Go Pathway analyses of proteins that were significantly decreased in muscle of both 4- and 12-week-old $Ryr1^{TM/SC-\Delta L}$ mice confirmed alterations in aminoacylation tRNA biosynthesis, sarco/endoplasmic
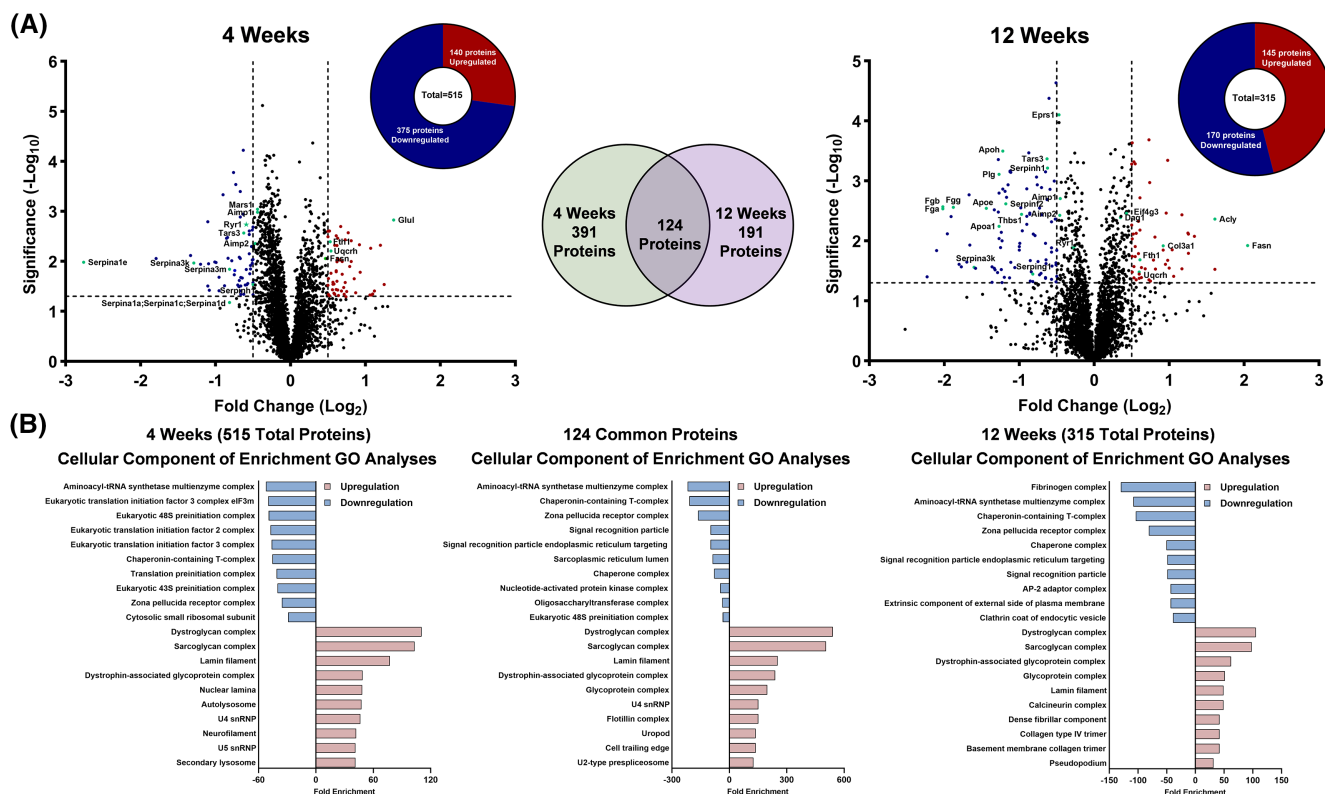
FIGURE 7 Proteomics analyses of *gastrocnemius* muscles from 4-week-old and 12-week-old $Ryr1^{+/+}$ and $Ryr1^{TM/SC-\Delta L}$ mice ($n=4$ for each group at each time point). (A) Donut charts showing the number of significantly upregulated and downregulated proteins and volcano plots of differential protein expression in *gastrocnemius* muscles from $Ryr1^{TM/SC-\Delta L}$ compared to $Ryr1^{+/+}$ mice at 4 weeks (*left*) and 12 weeks (*right*) of age. Significance cutoffs with a minimal Log$_2$ fold change set at ±0.5 are shown by vertical dashed lines, and $p=.05$ is shown by horizontal dashed lines. Proteins from top identified Cellular Component Enrichment Go Pathway analyses are highlighted. Venn diagram (*middle*) illustrates the overlap between significantly altered proteins observed in muscle from 4-week-old and 12-week-old $Ryr1^{TM/SC-\Delta L}$ and $Ryr1^{+/+}$ mice. (B) Cellular Component Enrichment Go Pathway analyses of significantly decreased (*blue*) and increased (*red*) proteins identified in muscles from $Ryr1^{TM/SC-\Delta L}$ compared to $Ryr1^{+/+}$ mice at 4 weeks of age (*left*), 12 weeks of age (*right*), and for protein changes observed at both ages (*middle*) ($n=4$ for each group at each time point).

reticulum and chaperone complexes (Figure 7B, *middle*), while the dystroglycan/sarcoglycan/DAG complexes and laminin filaments were the top altered pathways for proteins found to be increased in muscle of $Ryr1^{TM/SC-\Delta L}$ mice at both 4 and 12 weeks of age (Figure 7B, *middle*).

Of the 391 uniquely altered proteins in muscle of 4-week-old $Ryr1^{TM/SC-\Delta L}$ mice (112 upregulated and 279 downregulated), proteins involved in the autolysosome (Lamp1, Lamp2, and Gaa) were among the most upregulated, while ribosomal (Rpl12, Rpl3l, Rpl13a, and Rps11) and translation initiation (Eif2a, Eif3f, Eif4a2, Eif5b, and Eif4g3) proteins were among the most downregulated (Table 4). Consistent with these findings, Cellular Component Enrichment Go Pathway analyses identified translation (pre) initiation factors and cytosolic ribosomes as being the top altered pathways for proteins that were uniquely decreased in the muscle of 4-week-old $Ryr1^{TM/SC-\Delta L}$ mice. On the other hand, mRNA stability/splicing complexes, PKA complexes, autolysosomes, and secondary lysosomes were the top pathways identified for proteins

that were uniquely increased in muscle of 4-week-old $Ryr1^{TM/SC-\Delta L}$ mice (Figure S10, *left*). Of the 191 uniquely altered proteins in muscle of 12-week-old $Ryr1^{TM/SC-\Delta L}$ mice (105 upregulated and 86 downregulated), proteins involved in calcineurin signaling (Ppp3ca, Ppp3cb), extracellular matrix adhesion (Lamb1/2, Nid1), and basement membranes (Lamb1/2, Nid1/2, Anxa11, Col3a1, Col15a1, Col4a2) were among the most upregulated, while proteins involved in fibrinogen complex (e.g. Fga, Fgb, Fgg, Serpinf2, and Thbs1) and plasma lipoproteins (e.g. Apoe and Apoa1) were among the most downregulated (Table 5, Figure S10, *right*).

4 | DISCUSSION

Here, we generated the first compound heterozygous mouse model of severe, recessive RYR1-RM with non-identical missense mutations on separate $Ryr1$ alleles. Our aim was to recapitulate in a mouse model the phenotype

TABLE 3 List of common significantly altered proteins in muscle of both 4- and 12-week-old *Ryr1*$^{TM/SC-\Delta L}$ mice.

Proteins	Fold change (Log$_2$) at 4 weeks	Fold change (Log$_2$) at 12 weeks
Serpina3k	−1.29	−1.6
Rab3a	−0.76	−0.34
Afm	−0.66	−1.7
Ryr1;Ryr2	−0.63	−0.26
Tars3	−0.62	−0.63
Ryr1	−0.59	−0.27
Ahsg	−0.55	−0.9
Map2k6	−0.51	−0.44
Serpinh1	−0.5	−0.62
Gc	−0.49	−1.27
Aimp2	−0.47	−0.46
Mars1	−0.44	−0.38
Aimp1	−0.44	−0.45
Eprs1	−0.43	−0.47
Iars1	−0.4	−0.3
Tf	−0.4	−0.87
Colgalt1	−0.4	0.27
Hpx	−0.4	−1.28
Serping1	−0.37	−0.82
Rpl27a	−0.37	0.12
Srp72	−0.37	−0.26
Dars1	−0.37	−0.51
Edf1	−0.35	−0.35
Hdlbp	−0.35	−0.16
Eps15	−0.35	−0.34
C3	−0.35	−1.33
Fkbp4	−0.35	−0.5
Rab18	−0.34	0.53
Rab7a	−0.33	0.18
Kars1	−0.32	−0.31
Nt5c1a	−0.31	−0.52
Tmx2	−0.31	−0.73
Srp68	−0.31	−0.29
Lars1	−0.3	−0.2
Qars1	−0.3	−0.28
Cct4	−0.3	−0.26
Fam98a	−0.29	−0.23
Cct5	−0.29	−0.26
Prkaa2	−0.28	−0.23
Rars1	−0.28	−0.34
Cct6a	−0.28	−0.23
Tcp1	−0.28	−0.22
Cct8	−0.28	−0.3

(Continues)

TABLE 3 (Continued)

Proteins	Fold change (Log$_2$) at 4 weeks	Fold change (Log$_2$) at 12 weeks
Sqor	−0.28	−0.6
Cct3	−0.27	−0.22
Srp54	−0.27	−0.23
Cct2	−0.27	−0.27
Map2k3	−0.27	0.17
Cand2	−0.27	−0.4
Impdh2	−0.27	0.25
Rps20	−0.26	0.15
Carnmt1	−0.26	−0.47
Acsl6	−0.26	0.28
Rpl31	−0.26	0.1
Hsp90b1	−0.25	−0.29
Ica	−0.25	−0.9
Cct7	−0.24	−0.25
Farsa	−0.24	−0.25
Hook3	−0.24	−0.11
Ogt	−0.24	−0.36
Gyg1	−0.24	−0.13
Eef1g	−0.24	−0.12
Usp24	−0.23	−0.31
Tmem109	−0.23	−0.28
Gart	−0.23	−0.16
Sec31a	−0.23	−0.26
Farsb	−0.23	−0.29
Ppp1r3a	−0.22	−0.11
Rpn2	−0.22	−0.14
Prkab2	−0.22	−0.28
Bag2	−0.22	−0.36
Lman1	−0.22	−0.2
Glg1	−0.21	−0.47
Calr	−0.21	−0.21
Clasp1	−0.2	−0.24
Abhd16a	−0.19	−0.23
Apeh	−0.19	−0.44
Eef1a2	−0.19	−0.16
Eif3d	−0.19	−0.17
Fn1	−0.18	−0.96
Oat	−0.18	−0.14
Nqo2	−0.18	−0.26
Rpn1	−0.17	−0.2
Rab2a	−0.17	0.22
Rps23	−0.16	0.17
Eif3e	−0.16	−0.08
Pa2g4	−0.15	−0.12

(Continues)

TABLE 3 (Continued)

Proteins	Fold change (Log$_2$) at 4 weeks	Fold change (Log$_2$) at 12 weeks
Actr1a;Actr1b	−0.14	0.1
Cul3	−0.14	−0.31
Eef1a1;Eef1a2	−0.14	−0.17
Txnrd1	−0.14	−0.16
Slc41a3	−0.13	−0.51
Stip1	−0.12	−0.34
Ppp5c	−0.11	−0.19
Cul2	−0.11	−0.11
Isoc1	−0.09	−0.22
Cdh13	0.06	0.24
Sgca	0.12	0.21
Camk2d	0.14	0.4
Dmd	0.15	0.28
Col4a1	0.15	0.2
Nae1	0.16	0.25
Sgcd	0.17	0.3
Sgcg	0.19	0.27
Anxa4	0.2	0.55
Fbl	0.21	0.21
Dag1	0.21	0.35
Lmnb2	0.22	0.37
Bcap29	0.24	0.29
Pacsin3	0.24	0.36
Flot2	0.26	0.34
Snrpb;Snrpn	0.26	0.22
Sgcb	0.29	0.29
Cmas	0.3	0.37
Flot1	0.3	0.38
Acly	0.33	1.61
Lmnb1	0.37	0.27
Skp1	0.45	0.59
Fasn	0.47	2.05
Fth1	0.53	0.61
Uqcrh	0.54	0.6
Sorbs2	0.61	0.51
Uchl1	0.77	0.98
Glul	1.38	0.4

of a patient with recessive RYR1-RM due to co-inheritance of analogous missense *Ryr1* alleles from non-symptomatic parents. Similar to the family with these *RYR1* variants, we found that mice with only one of the mutant alleles, *Ryr1*$^{TM/+}$ and *Ryr1*$^{SC-ΔL/+}$ mice, lack an overt phenotype. Consistent with the clinical features of individuals with recessive RYR1-RM, including muscle weakness, hypotonia, respiratory dysfunction, and impaired ambulation,[28]

TABLE 4 List of unique significantly altered proteins in muscle of 4-week-old *Ryr1*$^{TM/SC-ΔL}$ mice.

Proteins	Fold change (Log$_2$) at 4 weeks
Bdh1	−1.01
Usp13	−0.90
Tfrc	−0.68
Klhl31	−0.67
Prkar1a	−0.63
Myo18b	−0.54
Mrps5	−0.51
Actg2	−0.50
Suclg2	−0.49
Carm1	−0.46
Nexn	−0.46
Phkb	−0.44
Msrb3	−0.43
Nek9	−0.40
Pfkm	−0.40
Chmp4b	−0.40
Arf2;Arf4;Arf5	−0.40
Mat2a	−0.40
Fxr1	−0.39
Palld	−0.39
Phka1	−0.38
Dnajc7	−0.38
Phkg1	−0.38
Pygm	−0.38
Txlnb	−0.37
Rcsd1	−0.36
Slc37a4	−0.36
Sar1b	−0.35
Rpl12	−0.35
Clic5	−0.35
Rpl3l	−0.35
Gphn	−0.34
Map2k2	−0.34
Cluh	−0.34
Rpl13a	−0.34
Pgam1;Pgam2	−0.33
Rpl6	−0.33
Agl	−0.33
Rpl14	−0.33
Mesd	−0.33
Oxct1	−0.33
Ldha	−0.32
Rps11	−0.32
Rrbp1	−0.32
Rpl5	−0.32
Rps4x	−0.32

TABLE 4 (Continued)

Proteins	Fold change (Log$_2$) at 4 weeks
Rpl13	−0.31
Rpl8	−0.31
Pygb;Pygl;Pygm	−0.31
Eif4a2	−0.31
Pkm	−0.31
Caprin1	−0.30
Rab12	−0.30
Tmod1	−0.30
Ubap2	−0.30
Rpl19	−0.30
Rplp0	−0.30
Rps18	−0.30
Eif5b	−0.30
Metap2	−0.29
Gls	−0.29
Rps12	−0.29
Rps2	−0.29
Rpl27	−0.29
Rps25	−0.29
Rpl23a	−0.29
Ndufaf1	−0.28
Rps3a	−0.28
Rpl26	−0.28
Eef2	−0.28
Rps10	−0.28
Rpl11	−0.28
Rab1A	−0.28
Pon3	−0.28
Slc25a4;Slc25a5	−0.28
Nme1;Nme2	−0.28
Naca	−0.28
Rpl10	−0.28
Creld1	−0.28
Rpl7a	−0.28
Fhod1	−0.27
Rpl9	−0.27
Rpl30	−0.27
Tars1	−0.27
Rpl24	−0.27
Rab1b	−0.27
Rpl35a	−0.27
Serbp1	−0.26
Rpl15	−0.26
Gcn1	−0.26
Ide	−0.26
Rps17	−0.26

(Continues)

TABLE 4 (Continued)

Proteins	Fold change (Log$_2$) at 4 weeks
Rpl17	−0.26
Lrpprc	−0.26
Rpl7	−0.26
Idh3b	−0.26
Ctps1	−0.26
Mat2b	−0.26
Idh3a	−0.26
Rpsa	−0.26
Atp2a1;Atp2a3	−0.26
Rps13	−0.26
Abcf2	−0.25
Ndufb10	−0.25
Trim54	−0.25
Rps9	−0.25
Usp47	−0.25
Myo18a	−0.25
Suclg1	−0.25
Dusp3	−0.25
Tmed7	−0.25
Suox	−0.25
Arcn1	−0.25
Upf1	−0.25
Arih1	−0.25
Lrpap1	−0.24
Kif1b	−0.24
Fam114a2	−0.24
Tpp2	−0.24
Rack1	−0.24
Lmod3	−0.24
Eif3f	−0.24
Rpl37a	−0.24
Eif3m	−0.24
Flii	−0.24
Eif2a	−0.24
Gbe1	−0.23
Rpl10a	−0.23
Emc3	−0.23
Ugp2	−0.23
Sec22b	−0.23
Sod2	−0.23
Synm	−0.23
Cacnb1	−0.23
Rps15a	−0.23
Eif2s2	−0.23
Rpl18a	−0.23
Rps8	−0.23

(Continues)

TABLE 4 (Continued)

Proteins	Fold change (Log$_2$) at 4 weeks
Mapkapk2	−0.23
Rabggta	−0.23
Rps19	−0.23
Rps7	−0.23
Homer1	−0.23
Eif3g	−0.22
Eif2s3x;Eif2s3y	−0.22
Sec23ip	−0.22
Tmx3	−0.22
Cpox	−0.22
Rps6	−0.22
Rps5	−0.22
Rps3	−0.22
Gpi	−0.22
Ndrg2	−0.22
Cacna1s	−0.22
Idh3g	−0.21
Copg1	−0.21
Maoa	−0.21
Ybx1	−0.21
Tst	−0.21
Arfgap2	−0.21
Rps14	−0.21
Rab21	−0.21
Ppp6c	−0.21
Pcyt2	−0.21
Rpl23	−0.20
Erap1	−0.20
Cops7a	−0.20
Samhd1	−0.20
Ckap5	−0.20
Usp4	−0.20
Sec13	−0.20
Dync1i2	−0.20
Eef1d	−0.20
Clip1	−0.20
Csde1	−0.20
Dnajb11	−0.20
Eif3b	−0.20
Pabpc1	−0.20
Etf1	−0.19
Mdh2	−0.19
Eif4a1;Eif4a2	−0.19
Ubap2l	−0.19
Eif3c	−0.19
Nudc	−0.19

TABLE 4 (Continued)

Proteins	Fold change (Log$_2$) at 4 weeks
Spr	−0.19
Chordc1	−0.19
Rab10	−0.19
Ubr4	−0.19
Abcf3	−0.18
Opa1	−0.18
Actr10	−0.18
Eif3l	−0.18
Fyco1	−0.18
Ipo7	−0.18
Eif3i	−0.18
Gpx4	−0.18
Eif3a	−0.18
Trim72	−0.18
Ykt6	−0.17
Ak3	−0.17
Cops6	−0.17
Psme2	−0.17
Anxa3	−0.17
Stt3b	−0.17
Stt3a	−0.17
Ethe1	−0.17
Eif2s1	−0.17
Dst	−0.17
Tmed2	−0.17
Vdac1	−0.17
Gps1	−0.16
Mapk14	−0.16
Lman2	−0.16
Rpl32	−0.16
Usp15	−0.16
Pabpc4	−0.16
Glrx3	−0.16
Strn3	−0.16
Eif4g2	−0.16
Ddx3x;Ddx3y	−0.16
Plin3	−0.16
Rheb	−0.16
Ddost	−0.16
Pcbp2	−0.16
Calu	−0.16
Actr1a	−0.15
Eif4g1	−0.15
Cops2	−0.15
Cops4	−0.15
Dnm1l	−0.15

TABLE 4 (Continued)

Proteins	Fold change (Log$_2$) at 4 weeks
Mybbp1a	−0.15
Eif1ax	−0.15
Uchl5	−0.15
Dnaja2	−0.15
Rab11b	−0.15
Atl2	−0.15
Ncln	−0.15
Gspt1;Gspt2	−0.14
Eef1b	−0.14
Unc45b	−0.14
Naa15	−0.14
Cars1	−0.14
Cisd1	−0.14
Prkcsh	−0.14
Cops5	−0.14
Ktn1	−0.13
Shmt2	−0.13
Ccdc47	−0.13
Eif3j1;Eif3j2	−0.13
Rab6a	−0.13
Ppp6r3	−0.13
P4hb	−0.13
Kpna1	−0.13
Hbs1l	−0.13
Psma6	−0.13
Erp44	−0.13
Hyou1	−0.13
Hectd1	−0.12
Ufl1	−0.12
Dctn1	−0.12
Sacm1l	−0.11
Dync1li1	−0.11
Emc2	−0.11
Psma2	−0.11
Psmd1	−0.11
Sars1	−0.11
Sec24c	−0.11
Mpi	−0.10
Dlg1	−0.10
Dnpep	−0.09
Rab14	−0.09
Usp9x	−0.09
Ppp2r2a	−0.09
Trap1	−0.09
Ddx6	−0.09
Psmb5	−0.09

(Continues)

TABLE 4 (Continued)

Proteins	Fold change (Log$_2$) at 4 weeks
Lnpk	−0.08
Psmc5	−0.07
Get3	−0.06
Fermt2	0.08
Wdr1	0.09
Ehd1	0.09
Limch1	0.09
Hnrnph1;Hnrnph2	0.10
Cavin1	0.10
Prkaca	0.10
Atp6v1a	0.10
Twf2	0.10
Nono	0.11
Tln1	0.12
Apex1	0.12
Itgb1	0.12
Alpk3	0.13
Srsf1	0.13
Snrnp200	0.13
Gsr	0.13
Alyref	0.14
Srsf7	0.14
Dbt	0.14
Tomm40	0.14
Fus	0.14
Stxbp3	0.14
Nop56	0.14
Prpf8	0.14
Por	0.15
Dhx9	0.15
Eftud2	0.15
Tom1	0.15
Lemd2	0.15
Lamp1	0.15
Ddx39b	0.15
Prkar2a	0.15
Trip10	0.16
Map3k20	0.16
Hnrnpm	0.17
Hnrnpu	0.17
Acad8	0.17
Gstz1	0.17
Myo1c	0.18
Cyb5r3	0.18
Esyt1	0.18
Cutc	0.19

(Continues)

TABLE 4 (Continued)

Proteins	Fold change (Log$_2$) at 4 weeks
Trim28	0.19
Itga7	0.19
Gcdh	0.19
Matr3	0.19
Khsrp	0.19
Akr1e2	0.19
Hspb8	0.20
Rps27a;Uba52	0.20
Tmpo	0.20
Adipoq	0.20
Prpf19	0.20
Ilk	0.21
Abra	0.21
Lbr	0.21
Hnrnpl	0.22
Hmgb1	0.23
Cenpv	0.24
Tpr	0.24
Ghitm	0.24
Ctsb	0.25
Hnrnpd	0.25
Lamp2	0.25
Thrap3	0.25
Camk2b	0.26
Fabp4	0.26
Pdcd6	0.27
Prune1	0.27
Septin11	0.27
Nup93	0.27
Ablim2	0.28
Lmna	0.28
Slc12a2	0.29
Bcat2	0.29
Emd	0.29
Tor1aip1	0.30
Scp2	0.30
Ctsd	0.30
Ppp2r5a	0.30
Aldh2	0.30
Myl6	0.32
Adhfe1	0.32
H4f16	0.32
Adh1	0.32
Ca3	0.32
Tkt	0.32
Sun1	0.34
Selenbp1	0.35

TABLE 4 (Continued)

Proteins	Fold change (Log$_2$) at 4 weeks
Actn1	0.36
Nxn	0.36
Mecp2	0.37
Anpep	0.38
Mylk	0.38
Gaa	0.38
Sorbs1	0.39
H1-0	0.42
Gpx3	0.42
Hp1bp3	0.47
Acox1	0.48
Fbln5	0.49
Akt2	0.50
Ablim1	0.59
Postn	0.59
Aoc3	0.63
Slmap	0.69
Mcpt4	0.85
Nefh	1.06
Plin1	1.07
Nefl	1.10
Ces1d	1.25

compound heterozygous $Ryr1^{TM/SC-\Delta L}$ mice exhibit significantly reduced Ryr1 protein expression, respiratory function, and locomotor activity, as well as muscle hypotrophy and weakness. Collectively, $Ryr1^{TM/SC-\Delta L}$ mice represent a valuable recessive RYR1-RM model resulting from the co-inheritance of two $Ryr1$ alleles with different missense mutations.

Several prior mouse models were developed to investigate the pathomechanisms of muscle dysfunction in recessive RYR1-RM. Of note, survival across these different recessive RYR1-RM models is highly variable, ranging from the birth lethality of $RYR1$ knockout (dyspedic) mice,[29] complete postnatal lethality of $Ryr1^{TM/Indel}$ mice,[11] to the absence of postnatal lethality for AD/Indel,[12] AD/AD[12] TM/TM[11], and FL/FL mice.[15] In recessive RYR1-RM patients, the degree of myopathy observed is generally associated with the relative degree of reduction in RYR1 protein expression.[2] Similarly, RYR1 expression is also related to the severity of myopathy and survival of recessive RYR1-RM mice. For example, Ryr1 protein expression in muscles of AD/Indel mice is approximately 60% of age-matched controls,[12] a reduction similar to that observed in tamoxifen-induced $Ryr1$ muscle-specific knock-down mice, where fatalities were also not reported.[14] In contrast, all $Ryr1^{TM/Indel}$ mice all die within 2 months after birth

TABLE 5 List of unique significantly altered proteins in muscle of 12-week-old *Ryr1*$^{TM/SC-\Delta L}$ mice.

Proteins	Fold change (Log$_2$) at 12 weeks
Fga	−2.02
Fgb	−2.02
Ighm	−1.96
Cfh	−1.91
Fgg	−1.88
Mug1	−1.77
Pzp	−1.67
Apoe	−1.44
Hrg	−1.27
Apoa1	−1.27
Plg	−1.27
Itih4	−1.24
Spta1	−1.24
Apoh	−1.22
Slc4a1	−1.20
Serpinf2	−1.18
Cp	−1.17
Ces1c	−1.15
Cfb	−1.12
Kng1	−1.12
Thbs1	−0.97
Ppid	−0.86
Itih2	−0.86
F2	−0.79
Serpinc1	−0.77
Hsph1	−0.76
Alb	−0.70
Oplah	−0.65
Ank1	−0.64
Blvrb	−0.64
Fubp1	−0.51
Trip12	−0.44
St13	−0.43
Rnpep	−0.43
Lcp1	−0.43
Hsp90aa1	−0.38
Mmab	−0.38
Fdps	−0.38
Fkbp3	−0.35
Cdc37	−0.34
Hspbp1	−0.33
Blmh	−0.32

TABLE 5 (Continued)

Proteins	Fold change (Log$_2$) at 12 weeks
Bcs1l	−0.31
Czib	−0.27
Fundc2	−0.26
Hagh	−0.26
Nudt2	−0.25
Pdxk	−0.25
Gsn	−0.25
Hsp90ab1	−0.24
Cdv3	−0.24
Pank4	−0.24
Hdhd2	−0.23
Hsp90aa1;Hsp90ab1	−0.23
Asph	−0.22
Myorg	−0.22
Bpnt1	−0.22
Mlf1	−0.22
Npepl1	−0.22
Hspa2;Hspa8	−0.21
Hspa8	−0.21
Ahsa1	−0.20
Nme2	−0.20
Macrod1	−0.20
Naa25	−0.20
Glod4	−0.19
Akr7a2	−0.19
Arpc3	−0.19
Grb2	−0.19
Pdia3	−0.19
Jph2	−0.19
Cul4a	−0.18
Prdx1	−0.18
Kpna3	−0.18
Hhatl	−0.16
Snx5	−0.16
Prps1	−0.16
Tbcb	−0.16
Glo1	−0.14
Ap2a1;Ap2a2	−0.14
Abcf1	−0.14
Plaa	−0.14
Memo1	−0.12
Blvra	−0.10
Synpo2l	−0.07

(Continues)

(Continues)

T A B L E 5 (Continued)

Proteins	Fold change (Log$_2$) at 12 weeks
Ppa1	−0.06
Syncrip	0.07
Dync1h1	0.08
Vapa	0.09
Gars1	0.09
Rsu1	0.10
Prep	0.12
Bcap31	0.12
Mypn	0.12
Wars1	0.13
Adss1	0.13
Pdcd5	0.14
Capza1	0.14
Otub1	0.15
Gpd1l	0.15
Qdpr	0.15
Lrrc47	0.15
Ncl	0.16
Sypl2	0.16
Ufd1	0.16
Mapk12	0.16
Gdi1;Gdi2	0.17
Arhgdia	0.17
Mpst	0.17
Prmt1	0.17
Gstm5	0.18
Aamdc	0.18
Tln2	0.18
Hspb2	0.20
Speg	0.20
Dcaf6	0.20
Comt	0.20
Mapk1;Mapk3	0.20
G3bp2	0.21
Lcmt1	0.21
Dtna	0.22
Alkbh3	0.22
Rps6kb2	0.22
Dpp3	0.22
Snta1	0.22
Hspb3	0.23
Ahcy	0.24
Hnrnpab	0.24

T A B L E 5 (Continued)

Proteins	Fold change (Log$_2$) at 12 weeks
Cobl	0.24
Phospho1	0.25
Plin4	0.25
Jph1	0.25
Eif4a1	0.25
Anxa11	0.26
Mylk2	0.26
Huwe1	0.26
Nid1	0.27
Hnrnpa3	0.27
Col4a2	0.27
Tceal5	0.27
Psmd14	0.27
Hdgf	0.27
Srl	0.27
Lama2	0.28
Pfn1	0.28
Lamc1	0.29
Tpt1	0.29
Nid2	0.30
Ppp3ca;Ppp3cb	0.30
Mapk1	0.30
Ddx5	0.30
Nploc4	0.30
Lamb1	0.31
Lpp	0.32
Txnl1	0.32
Eif4a3	0.33
Nt5c3a	0.33
Ddx17;Ddx5	0.33
Phykpl	0.33
Col15a1	0.35
Klhl40	0.35
Acaca;Acacb	0.37
Herc4	0.38
Akr1a1	0.39
Slc3a2	0.40
Pdlim3	0.40
Aarsd1	0.40
Eef1a1	0.40
Art3	0.41
Gfus	0.42
Eif4g3	0.43

T A B L E 5 (Continued)

Proteins	Fold change (Log₂) at 12 weeks
Alg2	0.44
Ranbp2	0.45
Rps6ka3	0.46
Sae1	0.46
Bsg	0.47
Xpnpep1	0.49
Tmem43	0.49
Ybx3	0.49
Dysf	0.50
Gpt2	0.51
Sms	0.51
Ppp3cb	0.52
Slc16a3	0.55
Fkbp5	0.61
Tsn	0.74
Pm20d2	0.75
Col3a1	0.92
Smyd2	0.98
Cnp	1.00
Rbm3	1.17

(despite significant supportive care) and exhibit ~80% reduction in RYR1 protein expression.[11] Therefore, the relative reduction in RYR1 protein expression in muscle is highly correlated with the mortality observed in multiple different recessive RYR1-RM mouse models.

In contrast to prior recessive RYR1-RM mouse models, compound heterozygous *Ryr1TM/SC-ΔL* mice exhibit a unique survival pattern. Specifically, *Ryr1TM/SC-ΔL* mice exhibit a smaller than expected birth rate (15% vs. 25%), followed by the progressive onset of incomplete postnatal mortality, ultimately resulting in a plateau of survival ~50% at 12 weeks of age (Figure 1A). To interrogate potential reasons for this unexpected bifurcation of survival, we quantified Ryr1 transcript and protein levels in TA muscle at two different postnatal timepoints: immediately before (4 weeks) and after (12 weeks) the observed changes in postnatal survival. We found that while *Ryr1* transcript level was not significantly different from WT at 4 weeks of age, Ryr1 protein expression was reduced to only ~25% of WT. We speculate that the reduction of Ryr1 protein at 4 weeks of age in the absence of change in *Ryr1* transcript could be due to the Ryr1 mutations resulting in misfolded subunits and/or unstable Ryr1 tetramers (in the absence of stabilizing WT subunits) that are then targeted for degradation. Consistent with this idea, our proteomic analyses found significant reductions in proteins involved in promoting

proper protein folding and chaperone complexes in muscle of 4-week-old (and 12-week-old) *Ryr1TM/SC-ΔL* mice. Alternatively, a reduction in the translational efficiency of *Ryr1* transcripts could also result in reduced Ryr1 protein expression. In contrast, both *Ryr1* transcript and protein levels were similarly reduced to ~60% of WT levels in TA muscle of *Ryr1TM/SC-ΔL* mice that survived to 12 weeks of age. Thus, in *Ryr1TM/SC-ΔL* mice that survive to 12 weeks of age, Ryr1 translation and protein stability processes establish a balance between steady-state *Ryr1* transcript and protein levels sufficient to support EC coupling, while limiting net overall SR Ca²⁺ leak through mutant RYR1 tetramers (see discussion below). Indeed, the level of Ryr1 protein expression in TA muscle during postnatal development generally mirrors changes in muscle weight (and body weight), as both postnatal muscle weight and Ryr1 protein expression increase in parallel from 4 to 12 weeks of age (Figure 1D,F). This correlation not only highlights the importance of Ryr1 protein expression during postnatal muscle growth, but also the importance of maintaining a proper balance between levels of RYR1 expression and Ryr1-dependent SR Ca²⁺ leak.

Three distinct mechanisms are proposed to explain how RYR1 disease mutations lead to reduced SR Ca²⁺ release and muscle weakness. One of the most widely recognized mechanisms ("RYR1 Ca²⁺ leak") involves the effect of *RYR1* mutations to promote SR Ca²⁺ leak. Specifically, a subset of mutations associated with malignant hyperthermia (MH) and central core disease (CCD) give rise to the formation of RYR1 Ca²⁺ release channels with different degrees of RYR1 Ca²⁺ leak.[30–38] In this case, the mutations result in RYR1 channels that are sensitized to activation due to the mutation either destabilizing the RYR1 channel closed state or stabilizing the channel open state.[19] With high levels of RYR1 Ca²⁺ leak, SR Ca²⁺ stores become partially depleted and resting Ca²⁺ is elevated due to increased steady-state Ca²⁺ entry via sarcolemmal channels.[39] A second mechanism ("EC uncoupling") involves RYR1 mutations that reduce the magnitude of voltage-gated Ca²⁺ release in the absence of enhanced RYR1 sensitization, SR Ca²⁺ leak, and store depletion.[32,40] This mechanism was first demonstrated for a pore mutation in the RYR1 pore (I4897T in rabbit RYR1)[33] that markedly reduces Ca²⁺ permeation.[19] However, an "EC uncoupling" mechanism could result from any mutation that results in: (1) disruption if proper RYR1 or DHPR junctional targeting, (2) mismatch in DHPR/RYR1 expression levels, (3) alteration in DHPR tetrad or RYR1 array assembly, (4) disruption in DHPR/RYR1 orthograde coupling, or (5) reduced RYR1 channel open probability and/or Ca²⁺ permeability.[41] The third mechanism for reduced SR Ca²⁺ release and muscle weakness is observed in

recessive forms of RYR1-RM in which RYR1 expression is markedly reduced, thus resulting in reduced SR release during muscle excitation.[42,43]

The skeletal muscle hypotrophy and weakness of $Ryr1^{TM/SC-\Delta L}$ mice appears to involve a combination of the three pathomechanisms described above. Consistent with reduced Ryr1 expression in FDB muscle of $Ryr1^{TM/SC-\Delta L}$ mice (Figure S1), we found that electrically evoked twitch stimulation results in a reduction in both Ca^{2+} release in FDB fibers (Figure 5). A similar reduction in twitch force generation was observed in EDL muscle of $Ryr1^{TM/SC-\Delta L}$ mice (Figure 3). In some muscles (e.g., *soleus* and *diaphragm* muscles of 12-week-old $Ryr1^{TM/SC-\Delta L}$ mice; Figure S1D,F), the marked reduction in Ryr1 expression results in a mismatch between Dhpr and Ryr1 expression levels, a form of EC uncoupling. Importantly, we also found that Ryr1 channels in $Ryr1^{TM/SC-\Delta L}$ mice exhibit greater Ca^{2+} leak/channel than that observed for age-matched WT mice. While the average maximum rate of SR Ca^{2+} leak was not significantly different in FDB fibers from 4-week and 12-week-old WT and $Ryr1^{TM/SC-\Delta L}$ mice (Figure 6), Ryr1 expression is reduced ~threefold in FDB muscle of $Ryr1^{TM/SC-\Delta L}$ mice at both ages (Figure S1A,D). Interestingly, we further found that SR Ca^{2+} leak for both genotypes is two- to threefold greater at 4 weeks of age compared to that observed at 12 weeks of age (compare Figure 6C,D). Thus, Ryr1 leak is reduced during postnatal development to a similar degree in muscle of both WT and $Ryr1^{TM/SC-\Delta L}$ mice. The reason for the greater rate of SR Ca^{2+} leak at 4 weeks is unclear, but may involve differences in Ryr1 post-translational modifications or interactions with other junctional proteins, which likely evolve during postnatal development. We speculate that the 50% of $Ryr1^{TM/SC-\Delta L}$ mice that survive to 12 weeks of age are able to properly balance Ryr1 mRNA and protein levels needed to maintain a normal level of Ryr1 Ca^{2+} leak, SR Ca^{2+} content, steady-state resting Ca^{2+} levels and still support robust Ca^{2+} release during EC coupling, while mice that are unable to accomplish this delicate balance die between 4 and 12 weeks of age.

Our finding that Ryr1 heterotetramers comprised of monomers of "TM" and "SC-ΔL" mutant subunits exhibit ~threefold greater Ca^{2+} leak per channel are consistent with prior single channel lipid bilayer studies conducted on purified Ryr1 channels following heterologous expression of the analogous mutations in human Ryr1 (TM and RC-ΔL). Specifically, these studies found that heterotypic Ryr1 channels comprised of mutant "TM" and "RC-ΔL" monomers exhibit an increased open probability even at low physiologic concentration (150 nM) of cytoplasmic Ca^{2+}.[18] This study also reported Fkbp12 dissociation from RYR1 in skeletal muscle from an RYR1-RM individual with the analogous RYR1 variants and that restoration of Fkbp12 binding to Ryr1 with a rycal (S107) stabilizes

the RYR1 channel closed state, thus reducing SR Ca^{2+} leak.[18] In contrast, we found that Fkbp12 remained associated with Ryr1 in TA muscle of $Ryr1^{TM/SC-\Delta L}$ mice. Interestingly, Magyar et al., 2023 reported that Ryr1 channels from skeletal muscle of homozygous TM/TM mice exhibit two functionally distinct populations of channels.[17] While one subset of homotypic mutant channels from TM/TM mice exhibited a relatively normal sensitivity to cytoplasmic Ca^{2+}, a second population of channels exhibited high open probability across all cytoplasmic Ca^{2+} concentrations tested (0.1–100 μM), consistent with a defect that would promote SR Ca^{2+} leak. It will be important for future studies to assess the cytoplasmic Ca^{2+} dependence of RYR1 channels purified from skeletal muscle of $Ryr1^{TM/SC-\Delta L}$ mice. Understanding the complex relationship and impact of enhanced RYR1 Ca^{2+} leak and reduced RYR1 protein expression on Ca^{2+} dynamics (e.g., SR Ca^{2+} cycling/store content, resting Ca^{2+}, electrically evoked Ca^{2+} release, sarcolemmal Ca^{2+} entry, etc) in skeletal muscle of $Ryr1^{TM/SC-\Delta L}$ mice will be needed to further unravel the mechanisms involved in the complex postnatal survival and phenotype of these mice.

The proteomic analyses in Figure 7 indicate that a reduction in proteins involved in protein synthesis (e.g., aminoacyl-tRNA synthetases, translation (pre)initiation factors, and ribosomal subunits) and an increase in proteins involved in the dystroglycan/sarcoglycan and DAG complexes reflect major protein changes in muscle of 4-week-old $Ryr1^{TM/SC-\Delta L}$ mice. Changes in protein translation (aminoacyl-tRNA synthetases) and folding/processing (chaperones) were among the top pathways observed for proteins that were significantly reduced in muscle of 12-week-old $Ryr1^{TM/SC-\Delta L}$ mice. Interestingly, an increase in proteins involved in the DAG complex (including dystrophin, dystroglycan, and multiple sarcoglycan isoforms) was the top upregulated pathway observed in $Ryr1^{TM/SC-\Delta L}$ mice at both 4 weeks and 12 weeks of age. This finding suggests that increased expression of proteins involved in coordinating a structural complex critical for maintaining sarcolemmal integrity during mechanical stress represents an important muscle adaptation of $Ryr1^{TM/SC-\Delta L}$ mice. Moreover, additional increases in proteins involved in the extracellular matrix (ECM) and basement membrane (e.g., Col3a1, Col15a1, Col4a2, Lamc1, Lamb1, Lama2, Nid1, Nid2, and Anxa11) were also observed in $Ryr1^{TM/SC-\Delta L}$ mice that survived to 12 weeks of age (Table 2, Figures 7B and S10). Thus, an upregulation of proteins of the ECM, basement membrane, and DAG complex may provide increased muscle membrane stability and integrity needed to limit muscle damage during postnatal development of $Ryr1^{TM/SC-\Delta L}$ mice.

Our proteomic analyses of *gastrocnemius* muscles from 12-week-old $Ryr1^{TM/SC-\Delta L}$ mice also revealed an

unexpected reduction in proteins involved in hemostasis (Fga, Fgb, Fgg, Serpinf2, and Thbs1) and plasma lipid particles (e.g., Apoe and Apoa1) (Figures 7 and S10). To determine if these alterations reflect a global change in blood cell composition, we quantified complete blood cell counts in whole blood from 12-week-old WT and $Ryr1^{TM/SC-\Delta L}$ mice (Figure S11). These analyses revealed no significant changes in blood cell numbers (white blood cells, lymphocytes, monocytes, neutrophils, red blood cells, or platelets) between the two genotypes. We speculate that the observed reduction in proteins involved in blood hemostasis and plasma lipid particles in muscle of 12-week-old $Ryr1^{TM/SC-\Delta L}$ mice reflects the markedly reduced size (~50%), and thus overall blood content, of whole muscles excised from $Ryr1^{TM/SC-\Delta L}$ mice.

A prior study completed comprehensive proteomic analyses of several different skeletal muscles (EDL, *soleus*, and extraocular) from 12-week-old WT and AD/Indel mice, a recessive model of RYR1-RM due to the co-inheritance of a missense variant allele (p.A4329D) coupled with a frameshift hypomorphic allele (p.Q1970fsX16).[44] Similar to that reported here for *gastrocnemius* muscles from $Ryr1^{TM/SC-\Delta L}$ mice, proteomic analyses also found a significant reduction in Ryr1 protein levels in EDL muscles from AD/Indel mice, as well as significant changes in proteins involved in protein synthesis, the extracellular matrix, and heat shock/chaperone proteins. In addition, similar to that reported by Eckhardt et al., we also found significant increases in calmodulin-dependent protein kinase delta in muscle of 4- and 12-week-old $Ryr1^{TM/SC-\Delta L}$ mice (see Table 5). In contrast, while muscles from 12-week-old AD/Indel mice exhibited decreased expression of collagen proteins and increased expression of chaperone proteins, muscles from 12-week-old $Ryr1^{TM/SC-\Delta L}$ mice exhibited increased expression of collagen proteins (Col3a1, Col15a1, and Col4a2) and decreased expression of chaperone proteins (Bag2, Calr, Sec31a, and Hsp90b1). Moreover, while an increase in ribosomal proteins was primarily observed in EDL muscles of AD/Indel mice, ribosomal proteins were mostly downregulated in muscle of $Ryr1^{TM/SC-\Delta L}$ mice and were not a major altered pathway in 12-week-old $Ryr1^{TM/SC-\Delta L}$ mice. Finally, we also observed an upregulation of proteins involved in fatty acid biosynthesis and the dystroglycan/sarcoglycan/DAG complexes in 12-week-old $Ryr1^{TM/SC-\Delta L}$ mice, but neither were reported as major altered pathways in AD/Indel mice. The reasons for these differences are unclear but could reflect the different fast twitch muscles used (EDL vs. *gastrocnemius*) or the fact that the $Ryr1^{TM/SC-\Delta L}$ mice exhibit a more severe myopathy as evidenced by their even smaller size and reduced postnatal survival.

In summary, this study describes the first mouse model of severe, recessive RYR1-RM due to co-inheritance of two non-identical missense *RYR1* alleles. Compound heterozygous mice exhibit a severe myopathy with incomplete (~50%) postnatal lethality that is characterized by a significant reduction in the expression of RYR1 channels with high levels of Ca^{2+} leak. Compensations that optimize Ryr1 expression/Ca^{2+} leak balance, enhance sarcolemmal stability, and promote fatty acid biosynthesis provide $Ryr1^{TM/SC-\Delta L}$ mice an increased survival advantage during postnatal development.

AUTHOR CONTRIBUTIONS

Robert T. Dirksen conceived the study; Chen Liang, Sundeep Malik, Miao He, Linda Groom, Sara K. Ture, Craig N. Morrell, and Robert T. Dirksen designed the experiments; Chen Liang and Robert T. Dirksen contributed to writing of the manuscript; Chen Liang, Sundeep Malik, Miao He, Linda Groom, and Sara K. Ture were responsible for data collection and analysis; Chen Liang, Sundeep Malik, Miao He, Linda Groom, Sara K. Ture, Craig N. Morrell, and Robert T. Dirksen were involved in data interpretation. All authors read and approved the final manuscript.

ACKNOWLEDGMENTS

FUNDING INFORMATION

DISCLOSURES

The authors declare no conflicts of interest.

DATA AVAILABILITY STATEMENT

The proteomic data that support the findings will be available in the centralized repository PRIDE (PRoteomics IDEntifications) database following an embargo from the date of publication to allow for commercialization of research findings. Other data that support the findings of this study are available in the Materials and Methods, Results, and/or Supplemental Material of this article.

ORCID

Chen Liang https://orcid.org/0000-0002-5562-350X
Miao He https://orcid.org/0000-0001-6094-7608
Sara K. Ture https://orcid.org/0000-0003-0568-8791
Robert T. Dirksen https://orcid.org/0000-0002-3182-1755

REFERENCES

1. Dulhunty AF, Wei-LaPierre L, Casarotto MG, Beard NA. Core skeletal muscle ryanodine receptor calcium release complex. *Clin Exp Pharmacol Physiol*. 2017;44(1):3-12. doi:10.1111/1440-1681.12676

2. Jungbluth H, Treves S, Zorzato F, et al. Congenital myopathies: disorders of excitation-contraction coupling and muscle contraction. *Nat Rev Neurol*. 2018;14(3):151-167. doi:10.1038/nrneurol.2017.191

3. Gonorazky HD, Bönnemann CG, Dowling JJ. The genetics of congenital myopathies. *Handb Clin Neurol*. 2018;148:549-564. doi:10.1016/b978-0-444-64076-5.00036-3

4. Amburgey K, Bailey A, Hwang JH, et al. Genotype-phenotype correlations in recessive RYR1-related myopathies. *Orphanet J Rare Dis*. 2013;8:117. doi:10.1186/1750-1172-8-117

5. Klein A, Lillis S, Munteanu I, et al. Clinical and genetic findings in a large cohort of patients with ryanodine receptor 1 gene-associated myopathies. *Hum Mutat*. 2012;33(6):981-988. doi:10.1002/humu.22056

6. Jungbluth H. Central core disease. *Orphanet J Rare Dis*. 2007;2:25. doi:10.1186/1750-1172-2-25

7. Clarke NF, Waddell LB, Cooper ST, et al. Recessive mutations in RYR1 are a common cause of congenital fiber type disproportion. *Hum Mutat*. 2010;31(7):E1544-E1550. doi:10.1002/humu.21278

8. Jungbluth H, Zhou H, Hartley L, et al. Minicore myopathy with ophthalmoplegia caused by mutations in the ryanodine receptor type 1 gene. *Neurology*. 2005;65(12):1930-1935. doi:10.1212/01.wnl.0000188870.37076.f2

9. Treves S, Jungbluth H, Muntoni F, Zorzato F. Congenital muscle disorders with cores: the ryanodine receptor calcium channel paradigm. *Curr Opin Pharmacol*. 2008;8(3):319-326. doi:10.1016/j.coph.2008.01.005

10. Wilmshurst JM, Lillis S, Zhou H, et al. RYR1 mutations are a common cause of congenital myopathies with central nuclei. *Ann Neurol*. 2010;68(5):717-726. doi:10.1002/ana.22119

11. Brennan S, Garcia-Castañeda M, Michelucci A, et al. Mouse model of severe recessive RYR1-related myopathy. *Hum Mol Genet*. 2019;28(18):3024-3036. doi:10.1093/hmg/ddz105

12. Elbaz M, Ruiz A, Bachmann C, et al. Quantitative RyR1 reduction and loss of calcium sensitivity of RyR1Q1970fsX16+A4329D cause cores and loss of muscle strength. *Hum Mol Genet*. 2019;28(18):2987-2999. doi:10.1093/hmg/ddz092

13. Elbaz M, Ruiz A, Nicolay S, et al. Bi-allelic expression of the RyR1 p.A4329D mutation decreases muscle strength in slow-twitch muscles in mice. *J Biol Chem*. 2020;295(30):10331-10339. doi:10.1074/jbc.RA120.013846

14. Pelletier L, Petiot A, Brocard J, et al. In vivo RyR1 reduction in muscle triggers a core-like myopathy. *Acta Neuropathol Commun*. 2020;8(1):192. doi:10.1186/s40478-020-01068-4

15. Benucci S, Ruiz A, Franchini M, et al. A novel, patient-derived RyR1 mutation impairs muscle function and calcium homeostasis in mice. *J Gen Physiol*. 2024;156(4):e202313486. doi:10.1085/jgp.202313486

16. Ruiz A, Benucci S, Duthaler U, et al. Improvement of muscle strength in a mouse model for congenital myopathy treated with HDAC and DNA methyltransferase inhibitors. *elife*. 2022;11:e73718. doi:10.7554/eLife.73718

17. Magyar Z, Hevesi J, Groom L, Dirksen RT, Almássy J. Function of a mutant ryanodine receptor (T4709M) linked to congenital myopathy. *Sci Rep*. 2023;13(1):14659. doi:10.1038/s41598-023-41801-2

18. Kushnir A, Todd JJ, Witherspoon JW, et al. Intracellular calcium leak as a therapeutic target for RYR1-related myopathies. *Acta Neuropathol*. 2020;139(6):1089-1104. doi:10.1007/s00401-020-02150-w

19. Loy RE, Orynbayev M, Xu L, et al. Muscle weakness in Ryr1I4895T/WT knock-in mice as a result of reduced ryanodine receptor Ca^{2+} ion permeation and release from the sarcoplasmic reticulum. *J Gen Physiol*. 2011;137(1):43-57. doi:10.1085/jgp.201010523

20. Smith LR, Barton ER. SMASH - semi-automatic muscle analysis using segmentation of histology: a MATLAB application. *Skelet Muscle*. 2014;4:21. doi:10.1186/2044-5040-4-21

21. Hakim CH, Li D, Duan D. Monitoring murine skeletal muscle function for muscle gene therapy. *Methods Mol Biol*. 2011;709:75-89. doi:10.1007/978-1-61737-982-6_5

22. Baylor SM, Hollingworth S. Sarcoplasmic reticulum calcium release compared in slow-twitch and fast-twitch fibres of mouse muscle. *J Physiol*. 2003;551(Pt 1):125-138. doi:10.1113/jphysiol.2003.041608

23. Capote J, Bolaños P, Schuhmeier RP, Melzer W, Caputo C. Calcium transients in developing mouse skeletal muscle fibres. *J Physiol*. 2005;564(Pt 2):451-464. doi:10.1113/jphysiol.2004.081034

24. Kimura T, Lueck JD, Harvey PJ, et al. Alternative splicing of RyR1 alters the efficacy of skeletal EC coupling. *Cell Calcium*. 2009;45(3):264-274. doi:10.1016/j.ceca.2008.11.005

25. Zvaritch E, Depreux F, Kraeva N, et al. An Ryr1I4895T mutation abolishes Ca^{2+} release channel function and delays development in homozygous offspring of a mutant mouse line. *Proc Natl Acad Sci USA*. 2007;104(47):18537-18542. doi:10.1073/pnas.0709312104

26. Lanner JT, Georgiou DK, Dagnino-Acosta A, et al. AICAR prevents heat-induced sudden death in RyR1 mutant mice independent of AMPK activation. *Nat Med*. 2012;18(2):244-251. doi:10.1038/nm.2598

27. Goedhart J, Luijsterburg MS. VolcaNoseR is a web app for creating, exploring, labeling and sharing volcano plots. *Sci Rep*. 2020;10(1):20560. doi:10.1038/s41598-020-76603-3

28. Lawal TA, Todd JJ, Meilleur KG. Ryanodine receptor 1-related myopathies: diagnostic and therapeutic approaches. *Neurotherapeutics*. 2018;15(4):885-899. doi:10.1007/s13311-018-00677-1

29. Takekura H, Nishi M, Noda T, Takeshima H, Franzini-Armstrong C. Abnormal junctions between surface membrane and sarcoplasmic reticulum in skeletal muscle with a mutation targeted to the ryanodine receptor. *Proc Natl Acad Sci USA*. 1995;92(8):3381-3385. doi:10.1073/pnas.92.8.3381

30. Avila G, Dirksen RT. Functional impact of the ryanodine receptor on the skeletal muscle L-type Ca(2+) channel. *J Gen Physiol*. 2000;115(4):467-480. doi:10.1085/jgp.115.4.467

31. Avila G, Dirksen RT. Functional effects of central core disease mutations in the cytoplasmic region of the skeletal muscle ryanodine receptor. *J Gen Physiol*. 2001;118(3):277-290. doi:10.1085/jgp.118.3.277

32. Avila G, O'Brien JJ, Dirksen RT. Excitation–contraction uncoupling by a human central core disease mutation in the

ryanodine receptor. *Proc Natl Acad Sci USA*. 2001;98(7):4215-4220. doi:10.1073/pnas.071048198

33. Avila G, O'Connell KM, Dirksen RT. The pore region of the skeletal muscle ryanodine receptor is a primary locus for excitation-contraction uncoupling in central core disease. *J Gen Physiol*. 2003;121(4):277-286. doi:10.1085/jgp.200308791

34. Avila G, O'Connell KM, Groom LA, Dirksen RT. Ca²⁺ release through ryanodine receptors regulates skeletal muscle L-type Ca²⁺ channel expression. *J Biol Chem*. 2001;276(21):17732-17738. doi:10.1074/jbc.M009685200

35. Lynch PJ, Tong J, Lehane M, et al. A mutation in the transmembrane/luminal domain of the ryanodine receptor is associated with abnormal Ca²⁺ release channel function and severe central core disease. *Proc Natl Acad Sci USA*. 1999;96(7):4164-4169. doi:10.1073/pnas.96.7.4164

36. Monnier N, Romero NB, Lerale J, et al. An autosomal dominant congenital myopathy with cores and rods is associated with a neomutation in the RYR1 gene encoding the skeletal muscle ryanodine receptor. *Hum Mol Genet*. 2000;9(18):2599-2608. doi:10.1093/hmg/9.18.2599

37. Tong J, Oyamada H, Demaurex N, Grinstein S, McCarthy TV, MacLennan DH. Caffeine and halothane sensitivity of intracellular Ca²⁺ release is altered by 15 calcium release channel (ryanodine receptor) mutations associated with malignant hyperthermia and/or central core disease. *J Biol Chem*. 1997;272(42):26332-26339. doi:10.1074/jbc.272.42.26332

38. Treves S, Larini F, Menegazzi P, et al. Alteration of intracellular Ca²⁺ transients in COS-7 cells transfected with the cDNA encoding skeletal-muscle ryanodine receptor carrying a mutation associated with malignant hyperthermia. *Biochem J*. 1994;301(Pt 3):661-665. doi:10.1042/bj3010661

39. Eltit JM, Ding X, Pessah IN, Allen PD, Lopez JR. Nonspecific sarcolemmal cation channels are critical for the pathogenesis of malignant hyperthermia. *FASEB J*. 2013;27(3):991-1000. doi:10.1096/fj.12-218354

40. Tilgen N, Zorzato F, Halliger-Keller B, et al. Identification of four novel mutations in the C-terminal membrane spanning domain of the ryanodine receptor 1: association with central core disease and alteration of calcium homeostasis. *Hum Mol Genet*. 2001;10(25):2879-2887. doi:10.1093/hmg/10.25.2879

41. Dirksen RT, Avila G. Altered ryanodine receptor function in central core disease: leaky or uncoupled Ca(2+) release channels? *Trends Cardiovasc Med*. 2002;12(5):189-197. doi:10.1016/s1050-1738(02)00163-9

42. Monnier N, Ferreiro A, Marty I, Labarre-Vila A, Mezin P, Lunardi J. A homozygous splicing mutation causing a depletion of skeletal muscle RYR1 is associated with multi-minicore disease congenital myopathy with ophthalmoplegia. *Hum Mol Genet*. 2003;12(10):1171-1178. doi:10.1093/hmg/ddg121

43. Zhou H, Yamaguchi N, Xu L, et al. Characterization of recessive RYR1 mutations in core myopathies. *Hum Mol Genet*. 2006;15(18):2791-2803. doi:10.1093/hmg/ddl221

44. Eckhardt J, Ruiz A, Koenig S, et al. Quantitative proteomic analysis of skeletal muscles from wild-type and transgenic mice carrying recessive Ryr1 mutations linked to congenital myopathies. *elife*. 2023;12:e83618. doi:10.7554/eLife.83618

SUPPORTING INFORMATION

Additional supporting information can be found online in the Supporting Information section at the end of this article.